



# Closing the water cycle from observations across scales: Where do we stand?

Wouter Dorigo <sup>a</sup>, Stephan Dietrich <sup>b</sup>, Filipe Aires <sup>c</sup>, Luca Brocca <sup>d</sup>, Sarah Carter <sup>e</sup>, Jean-François Cretaux <sup>f</sup>, David Dunkerley <sup>g</sup>, Hiroyuki Enomoto <sup>h</sup>, René Forsberg <sup>i</sup>, Andreas Güntner <sup>j,k</sup>, Michaela I. Hegglin <sup>l</sup>, Rainer Hollmann <sup>m</sup>, Dale F. Hurst <sup>n</sup>, Johnny A. Johannessen <sup>o</sup>, Chris Kummerow <sup>p</sup>, Tong Lee <sup>q</sup>, Kari Luojus <sup>r</sup>, Ulrich Looser <sup>s</sup>, Diego G. Miralles <sup>t</sup>, Victor Pellet <sup>u</sup>, Thomas Recknagel <sup>b</sup>, Claudia Ruz Vargas <sup>v</sup>, Udo Schneider <sup>w</sup>, Philippe Schoeneich <sup>x</sup>, Marc Schröder <sup>m</sup>, Nigel Tapper <sup>y</sup>, Valery Vuglinsky <sup>z</sup>, Wolfgang Wagner <sup>a</sup>, Lisan Yu <sup>al</sup>, Luca Zappa <sup>a</sup>, Michael Zemp <sup>bl</sup>, Valentin Aich <sup>cl</sup>

<sup>a</sup> TU Wien, GEO Department, Vienna, Austria

<sup>b</sup> International Centre for Water Resources and Global Change, German Federal Institute of Hydrology, Koblenz, Germany

<sup>c</sup> LERMA, CNRS/Observatoire de Paris, Paris, France

<sup>d</sup> National Research Council, Research Institute for Geo-Hydrological Protection, Perugia, Italy

<sup>e</sup> Wageningen University and Research, Laboratory of Geo-Information Science and Remote Sensing, Wageningen, The Netherlands

<sup>f</sup> Laboratoire d'Études en Géophysique et Océanographie Spatiales (LEGOS), Toulouse, France

<sup>g</sup> School of Earth, Atmosphere and Environment, Monash University, Melbourne, Australia

<sup>h</sup> National Institute of Polar Research, Tokyo, Japan

<sup>i</sup> National Space Institute, Technical University of Denmark

<sup>j</sup> Helmholtz Centre Potsdam GFZ German Research Centre for Geosciences, Potsdam, Germany

<sup>k</sup> University of Potsdam, Institute of Environmental Science and Geography, Potsdam, Germany

**Early Online Release:** This preliminary version has been accepted for publication in *Bulletin of the American Meteorological Society*, may be fully cited, and has been assigned DOI 10.1175/BAMS-D-19-0316.1. The final typeset copyedited article will replace the EOR at the above DOI when it is published.

- <sup>1</sup> *University of Reading, Department of Meteorology, Reading, United Kingdom*
- <sup>m</sup> *Satellite Climate Monitoring, Deutscher Wetterdienst, Offenbach, Germany*
- <sup>n</sup> *Cooperative Institute for Research in Environmental Sciences, University of Colorado, and NOAA Global Monitoring Division, Boulder, Colorado*
- <sup>o</sup> *Nansen Environmental and Remote Sensing Center and Geophysical Institute, University of Bergen, Norway*
- <sup>p</sup> *Colorado State University, Dept. Of Atmospheric Science, Fort Collins, Colorado*
- <sup>q</sup> *Jet Propulsion Laboratory, California Institute of Technology, Pasadena, California*
- <sup>r</sup> *Finnish Meteorological Institute, Helsinki, Finland*
- <sup>s</sup> *Global Runoff Data Centre, German Federal Institute of Hydrology, Koblenz, Germany*
- <sup>t</sup> *Hydro-Climate Extremes Lab (H-CEL), Ghent University, Ghent, Belgium*
- <sup>u</sup> *Institute of Industrial Science, The University of Tokyo, Tokyo, Japan*
- <sup>v</sup> *International Groundwater Resources Assessment Centre (IGRAC), Delft, The Netherlands*
- <sup>w</sup> *Global Precipitation Climatology Centre, Deutscher Wetterdienst, Offenbach a.M. Germany*
- <sup>x</sup> *University Grenoble Alpes, Institute for Urban Planning and Alpine Geography, Grenoble, France*
- <sup>y</sup> *School of Earth, Atmosphere and Environment, Monash University, Melbourne, Australia*
- <sup>z</sup> *Hydrological Institute, St. Petersburg, Russian Federation*
- <sup>al</sup> *Woods Hole Oceanographic Institution, Physical Oceanographic Department, Woods Hole, Massachusetts*
- <sup>b1</sup> *University of Zurich, Zurich, Switzerland*
- <sup>c1</sup> *Global Climate Observing System (GCOS), Geneva, Switzerland*

Corresponding authors: Wouter Dorigo, [wouter.dorigo@geo.tuwien.ac.at](mailto:wouter.dorigo@geo.tuwien.ac.at); Stephan Dietrich, [dietrich@bafg.de](mailto:dietrich@bafg.de)

## ABSTRACT

Life on Earth vitally depends on the availability of water. Human pressure on freshwater resources is increasing, as is human exposure to weather-related extremes (droughts, storms, floods) caused by climate change. Understanding these changes is pivotal for developing mitigation and adaptation strategies. The Global Climate Observing System (GCOS) defines a suite of Essential Climate Variables (ECVs), many related to the water cycle, required to systematically monitor the Earth's climate system. Since long-term observations of these ECVs are derived from different observation techniques, platforms, instruments, and retrieval algorithms, they often lack the accuracy, completeness, resolution, to consistently to characterize water cycle variability at multiple spatial and temporal scales.

Here, we review the capability of ground-based and remotely sensed observations of water cycle ECVs to consistently observe the hydrological cycle. We evaluate the relevant land, atmosphere, and ocean water storages and the fluxes between them, including anthropogenic water use. Particularly, we assess how well they close on multiple temporal and spatial scales. On this basis, we discuss gaps in observation systems and formulate guidelines for future water cycle observation strategies. We conclude that, while long-term water-cycle monitoring has greatly advanced in the past, many observational gaps still need to be overcome to close the water budget and enable a comprehensive and consistent assessment across scales. Trends in water cycle components can only be observed with great uncertainty, mainly due to insufficient length and homogeneity. An advanced closure of the water cycle requires improved model-data synthesis capabilities, particularly at regional to local scales.

## CAPSULE

By assessing the capability of available ground-based and remotely sensed observations of water cycle Essential Climate Variables, we discuss gaps in existing observation systems and formulate guidelines for future water cycle observation strategies.

## 1. Introduction

Life on Earth is intimately connected to the availability of water, to the point that when we search for life on other planets, we search for water. Its circulation through the hydrological cycle sustains the Earth's biosphere, which remains inherently vulnerable to the variability in water supply. With a steadily increasing world population and economic development, the demands on water resources and the potential damage by hydrometeorological extremes like droughts and floods are increasing too. But it is not only the hydrosphere that has impacted us, as vice versa, it is likely that human activities have influenced the global water cycle since mid-20th century (e.g. Bindoff et al. 2013; Marvel et al. 2019; Padrón et al. 2020; Bonfils et al. 2020). However, observational uncertainties in combination with strong natural climate variability render estimates of the human contribution to recent trends uncertain, and overall challenge the detection and attribution of change, in particular with regard to extremes and local phenomena (Hegerl et al. 2015; National Academies of Sciences 2016).

The Paris Agreement of the UNFCCC also addresses these observational needs and demands that “*Parties should strengthen [...] scientific knowledge on climate, including research, systematic observation of the climate system and early warning systems, in a manner that informs climate services and supports decision-making*” (United Nations 2015). The call of the UNFCCC for enhancing systematic observations expresses the need for climate monitoring based on best available science, which is globally coordinated through the Global Climate Observing System (GCOS). In the current Implementation Plan of GCOS,

main observation gaps are addressed and it states that “*closing the Earth's energy balance and the carbon and water cycles [...] through observations remain outstanding scientific issues that require high-quality climate records of ECVs*” (GCOS 2016). Water-related ECVs are specified by GCOS and critically contribute to the characterization of Earth’s climate including the global water cycle (Bojinski et al. 2014).

#### *a. Components of the water cycle*

The water cycle, also known as the hydrological cycle, describes the continuous movement of water between storages at, above, and below the Earth's surface (Figure 1 Observed estimates of global water cycle storages (in  $10^3 \text{ km}^3$ ) and their uncertainties. Sources of individual estimates are reported in Table 1. and Figure 2). We summarize status and long-term changes trends of both, the changes in storage but also changes in fluxes, respectively. Storages include water bodies (oceans, seas, lakes, rivers, artificial reservoirs), atmospheric water (water vapor, clouds), subsurface water (soil moisture, groundwater), frozen water (glaciers, ice sheets, sea ice, snow, ground ice) and the biosphere as a whole. The key fluxes linking these storages include:

- Terrestrial and surface water evaporation and sublimation;
- Precipitation, either in liquid, gas, or frozen state;
- Uptake and release by the cryosphere, lakes and artificial reservoirs, and aquifers;
- Surface water runoff and flow;
- Recharge and depletion of water bodies by humans;

On a yearly basis, only about 0.008% of the water available on Earth is cycled (Oki and Kanae 2006). In other words, theoretically, it takes about 12,500 years until all water molecules have completed a full ocean–atmosphere–land–ocean cycle.

The largest water cycle fluxes take place over the ocean: The ocean produces about 87% of the global evaporation and receives approximately 78% of the global precipitation (Baumgartner and Reichel 1975; Oki and Kanae 2006). The imbalance implies a net moisture transport from the ocean to the continents through the atmosphere, making the ocean an important source of continental precipitation (Trenberth et al. 2011; Gimeno et al. 2012). The net transport of freshwater from the ocean to the continents through the atmosphere is compensated by river discharge. Other runoff sources, such as annual snow and ice melt and groundwater flow into the ocean are estimated to be less than 10% of the river discharge (Burnett et al. 2001).

*b. Human impacts on the water cycle*

Nowadays, nearly all components of the water cycle are directly or indirectly influenced by humans (Abbott et al. 2019). Direct anthropogenic impacts include the extraction of ground or surface water for agricultural, domestic, or industrial purposes or the construction of reservoirs. However, indirect changes, caused by human-induced global warming or land use and land cover change, have possibly even further-reaching consequences. Rising temperatures impact the cryosphere by causing the decline of glaciers and ice sheets (Zemp et al. 2019), by shortening the snow-covered season in alpine areas and northern latitudes (Pulliainen et al. 2020), and by exacerbating sea ice melt. The resulting changes in albedo have shown to lead to more stable weather patterns, thus influencing the distribution of precipitation in space and time (Doughty et al. 2012). At a more local scale, a change to more rain and less snow in montane catchments in a warmer future may have severe implications for seasonal water availability (e.g. Singh and Bengtsson 2004; Berghuijs et al. 2014). Discharge is expected to peak in some catchments as glacier melt swells rivers before declining as glacier mass reduces in a warming climate (e.g. Pritchard 2019; Allan et al. 2020).

Anthropogenic global warming increases the water holding capacity of the atmosphere, with consequences for evaporation and precipitation patterns over ocean and land (See Sidebar). It is expected that in a warmer world extreme precipitation events will deliver a larger proportion of total annual precipitation (Fowler et al., 2021, Pfahl et al., 2017). This may impact many water cycle processes, including increased surface runoff, and more variable rainfall arrival may reduce water security (Eekhout et al. 2018). Simultaneously, an increase in large rainfall events may beneficially enhance groundwater recharge, particularly in dry climates, where major rainfall events are frequently required to trigger groundwater recharge (Thomas et al. 2016). Precipitation is also subject to modification if the condition of the land surface is altered: large-scale loss of tropical forests may cause rainfall change via reduced and seasonally changed plant transpiration and the altered precipitation recycling that can result (Ellison et al. 2017; Peña-Arancibia et al. 2019). Changes in land surface conditions may also affect large-scale temperature gradients and thus circulation and moisture advection (Zhou et al. 2021).

There is also strong evidence of clear links between global warming, evaporative demand and the promotion of drought and aridity (Zhou et al. 2019a; Williams et al. 2020; Vicente-Serrano et al. 2020), but the strength of these relationships varies regionally and seasonally (Cook et al. 2020a). Conversely, Cook et al. (2020b) have shown that large-scale expansion and intensification of irrigation has buffered warming trends in some regions, but it is not certain if these trends will persist under future climate change conditions. A reduction in relative humidity over land is a particularly strong climate change signal in both observations and model results and has been clearly linked to warming over neighboring oceans (Byrne and O’Gorman 2016, 2018).

Agricultural production, especially from irrigation as noted above, alters evaporative fluxes from the land surface. The net effect of raising atmospheric CO<sub>2</sub> levels on plant

physiology and the water cycle are still uncertain. On the one hand, CO<sub>2</sub> fertilization may cause increased water use efficiency and suppress plant transpiration (Gedney et al. 2006, Berg and Sheffield 2019) resulting in higher maximum daily temperatures (Lemordant and Gentine 2019) with an additional possible feedback to evaporation, but also allows greater retention of soil moisture, and larger runoff ratios during rainfall (e.g. Idso and Brazel 1984; Kooperman et al. 2018). On the other hand, enhanced transpiration losses associated with CO<sub>2</sub>-driven greening may lead to reduced streamflow (Ukkola et al. 2016).

### *c. Observing the water cycle*

The Earth's water cycle is monitored through three pillars – *in situ* observations, satellite observations, and observation-driven modelling. GCOS has currently defined a set of 54 ECVs, which are variables that are fundamental for monitoring the state of the climate and from an observational perspective mature enough to provide long-term consistent measurements in a systematic way (Bojinski et al. 2014; GCOS 2016). Especially over land, *in situ* data provide long-term records of the different components of the water cycle (see A1 and A2). Global *in situ* data centers, often operating under the auspices of UN organizations, collect globally available water data, harmonize them, and make them again publicly available. For some variables (e.g., precipitation and river discharge), time series from *in situ* observations are long enough (>30 y) to allow for detection of climate trends and variability but for most variables (e.g., evaporation over ocean and land), records are much shorter. Moreover, *in situ* data are sparse and, depending on the variable and process, representative only for a limited spatial domain. The shorter the time series, the more difficult it becomes to separate climate change signals from natural variability and changes caused by direct human interference in the water cycle.

Over the last four decades, the amount of relevant satellite-derived hydrological variables has significantly increased (Rast et al. 2014), and programs like ESA's Climate Change



Initiative (Hollmann et al. 2013) have promoted the combination of water cycle observations from multiple satellites into long-term Climate Data Records (CDRs) (Appendix Tables A1, A2). The recent expansion of operational missions (e.g., Copernicus Sentinels, EUMETSAT Metop, NOAA JPSS) jointly with innovative explorer satellites (e.g., GPM, GRACE(-FO), Aeolus, SMOS, SMAP, SWOT) is improving our observational capacity, while methodological progress such as artificial intelligence reduces retrieval errors and improves uncertainty descriptions. Nonetheless, observing subtle climate change signals like extreme events, and adequately characterizing errors of the observations remains challenging.

Reanalysis systems assimilate a broad array of observations into atmosphere, ocean, and land models to compute a suite of prognostic variables (e.g. Hersbach et al. 2020). Reanalyses are particularly important for studying water cycle variability, since they aim to provide complete and continuous information. However, self-consistency in reanalyses is not guaranteed (Albergel et al. 2013; Trenberth et al. 2011). Issues arise from the heterogeneous mix of assimilated observations (which exhibit varying spatial and temporal representativeness and accuracy), as well as systematic biases in the modelling system itself (Bosilovich et al. 2017). Although the latest generation of reanalysis products, e.g., MERRA-2 or ERA5, show improvements over their predecessors, trends in many of their water cycle components remain uncertain (Bosilovich et al. 2017; Hersbach et al. 2015; Yu et al. 2020). Besides, global scale changes are particularly difficult to capture in reanalyses since the moisture and energy balances are not constrained. While atmospheric moisture variability has been much improved in the latest generation reanalysis products, global mean changes in precipitation are still not captured. Thus, global-scale water cycle trends in general are unrealistic in reanalysis products (Allan et al., 2020).

*d. Recent state of water budget closure and imbalance*

Because of the large variety of observation platforms, methodological approaches, and scientific communities involved, current observed water cycle ECVs are in imbalance, meaning that when adding up all components, water is added to or removed from the global cycle (Sheffield et al. 2009; Luo et al. 2021; Abolafia-Rosenzweig et al. 2021). Popp et al. (2020) proposed a set of rules to improve consistency between CDRs but further research and development, e.g., on ECV interdependencies at the retrieval and scientific levels, is needed to achieve this goal for observed water cycle components. There is also the problem of missing variables pertinent to the closure of the water cycle that cannot be readily observed but have to be obtained from observation-driven modelling, e.g., atmospheric water vapor transport from ocean to land, infiltration.

Based on the state-of-the-art of existing datasets and challenges ahead, GCOS defined observation targets for each individual ECV and for closing the water cycle including associated uncertainty estimates on annual time scales (GCOS 2016). The GCOS target for closing the global water cycle is within 5% annually, but without being backed up by a solid argument. In theory, the CDRs currently available should be sufficient to achieve this target and, indeed, in the majority of cases, the observed annual surface and atmospheric water budgets over the continents and oceans close with much less than 10% residual (GCOS 2015). Posing additional closure constraints allows to further reduce the errors of the individual variables (Pellet et al. 2019).

Even if annual closure within 5% uncertainty can be attained, this does not necessarily allow for monitoring water cycle variability in all its facets. Appropriate climate monitoring also requires consistency at sub-annual time scales (e.g., seasonal, monthly, or shorter) to monitor changes in extremes like storms, floods, heatwaves, and droughts (Koutsoyiannis 2020). For these time scales, observed residuals and optimized uncertainty estimates are considerably larger, often nearing or exceeding 20% (Rodell et al. 2015). Moreover, even at

the time scale of only a few decades average storages and fluxes are not static, since human-induced global warming and direct intervention in the Earth system have substantial impact on each of the terms (Wada et al. 2012). Thus, apart from water cycle closure at short time scales, also the sum of all trends needs to close (e.g. Stephens et al. 2012; Allan et al. 2020; Gutenstein et al. 2021; Thomas et al. 2020)

The goal of this paper is to provide a holistic review of available global long-term land, atmosphere, and ocean water cycle storage (section 2) and flux (section 3) products from *in situ* and Earth observations. Reanalysis data are only discussed if direct observations are impossible. In particular, supported by a review on existing water cycle closure studies, we evaluate how well these products perform in closing the water cycle at multiple temporal (annual, monthly, multi-decadal) and spatial (global, basin, pixel) scales (section 4). Based on the review, we discuss gaps in existing observation systems and formulate guidelines for future water cycle observation strategies for implementation in GCOS (section 5). While in section 2 and 3 we focus on the storages and fluxes one by one, we synthesize the common benefits, limitations or difficulties in section 5.

## **2. Observing Water Cycle Storages**

### *a. Ocean (fresh)water storage*

Oceans contain 96.5% of the water on Earth (Eakins and G.F. Sharman 2010), taking into account water volume in the upper 2 km of the Earth's crust. Observations of global mean sea level (GMSL) can be used to infer the change of ocean freshwater storage after removing the effect of thermal expansion and glacial isostatic adjustment.

Tide gauge networks date back to the late 19th century and are sparsely distributed along the coasts, which is a major factor contributing to the uncertainty of the estimated change of GMSL. Historical ocean temperature measurements have been used to estimate the thermal

expansion of the global ocean through time (e.g. Levitus et al. 2012; Ishii et al. 2017), however, much of the historical ocean temperature measurements had been in the upper few hundred meters and sparsely distributed along ship tracks. The development of the Argo profiling floats since the mid-2000s have enabled a near-global array of Argo floats that sample the ocean down to a depth of 2000 m. Full-depth Argo floats are being developed, complementing the full-depth ship-board hydrographic measurements from research vessels.

Satellite altimeters have revolutionized the study of GMSL change by providing full global coverage since the 1990s. Satellite measurements from GRACE(-FO) have provided reliable estimates of the change of global ocean mass from 2003 onward, although this record is likely too short to characterize the long-term trend (Blazquez et al. 2018).

b. Lakes and artificial reservoirs Lakes range in size from small ponds to inland seas. Their geographical distribution is very irregular, while most are located at high latitudes in formerly glaciated areas of the northern hemisphere (Downing et al. 2006; Williamson et al. 2009). Reservoirs are water bodies with artificial regulation of water reserves. Most reservoirs are constructed for hydropower purposes, but smaller ones exist for irrigation purposes.

Water volume (change) is estimated from water level observations using a so-called volume curve, which describes the relationship between water level and the corresponding water volumes based on the lake's or reservoir's morphology. For many large lakes, such volume curves are available but need to be regularly updated due to changes in the morphometric characteristics over time. For reservoirs, these curves are computed in the design phase and regularly updated in connection with the sedimentation of reservoirs. *In situ* observations of lake water level are usually carried out by national hydrological networks, adopting the standards prescribed by WMO. Thus, most *in situ* observations of lake water level are globally consistent and have accuracies of  $\pm 1$  cm (WMO 2008). Long-term

sampling efforts have primarily focused on northern temperate sites, while observations are scarce in many other areas, including remote, lake-rich regions in the Canadian and Siberian (sub-)arctic, less-populated areas like the Himalayas and the Andes, and populated regions like the African Great lakes.

Despite being less accurate than in situ observations, current satellite altimeters provide dense measurement time series of water surface elevation for the largest lakes, and optical and radar observations of lake area. Water volume (change) of a large number of lakes can thus be inferred from the combination of satellite observations of water level and extent (Gao et al. 2012; Busker et al. 2019; Crétaux et al. 2016). Water height and extent observations collected at different epochs can be used to build hypsometry relationships between height and volume changes in order to obtain water volume variations from water heights measured by satellite altimetry (Crétaux et al. 2016).

### *c. Atmospheric moisture*

The atmosphere is one of the smallest storages for water within the water cycle (Trenberth et al. 2007; Gleick 1996). Regionally, seasonal and inter-annual variations in atmospheric moisture are driven by changes in the distribution of sources (evaporation), sinks (precipitation), and the moisture flux convergence (e.g. Oki 1999). Under steady-state assumptions, the large sources and sinks lead to a short ( $8.9 \pm 0.4$  days) global average residence time for atmospheric water (van der Ent and Tuinenburg 2017). Yet despite the small storage capacity of the atmosphere, atmospheric transport is the rate-limiting step in moving water ‘upstream’ from oceans to land. It is noteworthy that this transport constitutes only 10% of the oceanic evaporation source.

Atmospheric moisture is measured by a wide variety of ground-based, balloon- and aircraft-borne, and satellite instruments. A near-global network of sites launching balloon-

borne radiosondes has provided high-resolution vertical profiles of relative humidity (RH) since the mid-1940s (Stickler et al. 2010), but only a few stations provide reliable long-term records for climate trend analysis (Wang and Zhang, 2007; Ferreira et al. 2019). Balloon-borne frost point hygrometers provide high-resolution, high-quality profiles of water vapor number density up to the middle stratosphere, but soundings are sparse in space and time. Ground-based microwave radiometers, LIDARs, FTIRs and GPS receivers provide coarser resolution profiles. Routine, high-quality RH measurements are made from commercial aircraft (Brenninkmeijer et al. 2007; Petzold et al. 2015; Moninger et al. 2010).

Satellite observations of atmospheric moisture (Schröder et al. 2016; Hegglin et al. 2013; Willett et al. 2020) offer near-global coverage, show steady quality and coverage improvements since the late 1970s, and are the main source of measurements over the oceans and developing countries where high-quality *in situ* measurements are scarce. Nadir-viewing sensors can provide coarse-resolution vertical profiles (e.g. Schröder et al. 2016). Limb-viewing sensors have higher vertical resolution, but are limited mostly to measurements above the middle troposphere (e.g. Hegglin et al. 2013). Nadir-viewing satellite microwave instruments have provided TCWV retrievals, mostly over oceans, since the late 1980s. The SSM/I-based data records exhibit consistent results in tracking changes in precipitable water vapor over the ice-free ocean (e.g., Schröder et al., 2016) and, when combined with ERA5 over remaining regions, can be used to analyse global trends (e.g., Allan et al. 2020) .

Nadir-viewing infrared sounders date back to the early 1980s (radiometers) and 2000s (spectrometers with higher accuracy and vertical resolution). Infrared instruments measure over both ocean and land but are limited to (near-)clear sky views, while near-infrared retrievals are limited to over-land and clear-sky views. Finally, high-accuracy GPS radio-occultation profile measurements are routinely made in all weather conditions since 2001 (Wickert et al., 2001).

#### d. Soil moisture

Soil moisture strongly interacts with highly dynamic major water and energy fluxes, importantly precipitation, evaporation, and runoff. Therefore, observing systems must be capable of capturing soil moisture dynamics at their native process scales, which is from sub-daily to 10-daily time steps, and from tens of meters to tens of kilometers, depending on the considered soil depth and climatic process studied.

The first systematic soil moisture measurements were taken in the 1950s in the former Soviet Union (Robock et al. 2000). Today, many countries, organizations, and individual scientists freely share their *in situ* soil moisture measurements, most importantly via the International Soil Moisture Network (Dorigo et al. 2021, 2013). Yet, most stations are in economically developed regions with temperate climatic conditions and have limited temporal coverage (most stations were established after 2000). Besides, nearly all networks have their unique purpose, design, measurement setup, and representativeness errors, which complicates their use to predict soil moisture at larger scales (Gruber et al. 2013; Dorigo et al. 2021).

Microwave remote sensing satellites have provided a growing number of global soil moisture data sets since the beginning of this century. Global soil moisture data sets are operationally provided for several passive and active microwave missions (Entekhabi et al. 2010; Kerr et al. 2012; Wagner et al. 2013) and many of them are fused into global long-term (Gruber et al. 2019; Dorigo et al. 2017) or near-real-time (Yin et al. 2019) multi-satellite products. The spatial resolution of these soil moisture datasets ranges between 10 and 50 km, and the temporal sampling is 1 to 3 days. The native satellite soil moisture products can only provide information about the soil moisture conditions in the top few centimeters of the soil, but model-data integration and infiltration models can be used to estimate the water content in the root zone (Ford et al. 2014; Babaeian et al. 2019). Estimates of deeper soil layers

remain unobserved while their skill reduces for dense vegetation (Dorigo et al. 2010). Although in many areas satellite soil moisture observations are still outperformed by reanalysis products, they start to converge and, in many areas, provide complementary skill (Beck et al. 2021; Dorigo et al. 2017).

#### *e. Groundwater*

Groundwater is by far the Earth's largest liquid freshwater storage (Gleeson et al. 2016), and supports about one third of human water use (Wada et al. 2014). Its widespread non-sustainable use has led to a depletion of aquifers in many regions worldwide (Famiglietti 2014).

Traditionally, groundwater level is monitored by *in situ* observations in boreholes or wells and many countries operate a national groundwater monitoring network. (e.g. Hosseini and Kerachian 2017). As setting up and maintaining the networks is costly, groundwater records are often sparse, short, or discontinuous and thus poorly suitable for climate studies. This is further complicated for observations in confined aquifers or those affected by human withdrawals, and by restrictive data sharing policies. The latter also hampers initiatives to combine observations to provide an overview of changes in groundwater levels at a global scale, such as pursued by the Global Groundwater Monitoring Network. Converting the observed head variations into regional groundwater storage variations involves considerable uncertainty from poorly known storage coefficients or specific yield values (Chen et al. 2016), site-specific dynamics (Heudorfer et al. 2019), or management-driven clustering of observation wells in highly productive aquifers while neglecting others.

Since April 2002, GRACE and GRACE-FO provide estimates of the Earth's variations of total terrestrial water storage (TWS) with at least monthly resolution. After removing from TWS the signal components that are not due to groundwater (i.e., soil moisture, surface



waters, snow and ice), it allows for monitoring groundwater storage dynamics (e.g. Rodell et al. 2018). Limitations of satellite gravimetry for monitoring groundwater dynamics are its coarse spatial resolution (>200 km), the necessary filtering of the raw data to remove noise at the expense of attenuation and spatial smoothing (leakage), and the uncertainties in usually model-based estimates of other mass variations (Chen et al. 2016).

Beyond recent progress with dynamic, gradient-based groundwater models at the global scale (de Graaf et al. 2015; Reinecke et al. 2019), there have been numerous developments on assimilating GRACE-based TWS into land surface and hydrological models with simple groundwater schemes. This allows for separating TWS into its compartments for individual river basins and aquifers, and recently also globally (Li et al. 2019). Results tend to indicate that GRACE data assimilation improves the simulation of groundwater storage variations as long as human groundwater withdrawal schemes are part of the model structure.

#### *f. Permafrost and ground ice*

Permafrost is defined as subsurface material with temperatures constantly below 0°C. Relevant for the water cycle is the so-called “ice-rich permafrost”, which covers huge areas in Arctic countries and the Tibetan Plateau. Ice-rich permafrost in mountain areas is mostly found in frozen scree slopes, rock glaciers and relict ice bodies. Most of the ground ice is perennial, but the upper decimeters to meters are subject to seasonal thaw and refreeze cycles, thus playing a role in the yearly water cycle. Likewise, the permanent melting of permafrost due to global warming adds water to the transient part of the water cycle.

Permafrost cannot be directly mapped and its distribution, ice richness, and volumes are extrapolated from available ground borehole observations using models. The most up-to-date estimates of the total amount of ice stored in Northern Hemispheric permafrost stem from Zhang et al. (2000, 1999), and are based on the *Circum-arctic map of permafrost and ground*

*ice conditions* (Brown et al. 2002; Heginbottom et al. 1993), with assumptions on total area, thickness, and mean ice-content. Permafrost is present also in ice-free areas of Antarctica, but there is no available estimation of its ice-volume.

Ice content of permafrost in rock glaciers is usually estimated through geophysical methods, but more precise quantification can only be achieved by boreholes. Due to large costs and logistical and technical difficulties these are extremely rare. A global estimation of ice content in rock glaciers was achieved from a rock glacier inventory and the use of a standard area/thickness relationship and assumptions on the ice content (Jones et al. 2018). This does not include dead ice bodies from glacial origin that can remain over centuries or millennia in periglacial conditions, and which are considered neither in glacier nor in rock glacier inventories.

Changes in permafrost water storage are due essentially to the deepening of the active layer, which induces melting of ice at the top of the perennially frozen ground and its restitution to the water cycle. Observations of the active layer thickness only partly account for ice volume loss, as land surface subsidence (remotely sensed with ground validation) need to be considered too.

#### *g. Snow*

Terrestrial snow is characterized by high spatial and temporal variability and until very recently, snow has been one of the more uncertain components of the water cycle, particularly in mountain areas (Lievens et al. 2019).

Various terrestrial snow parameters have been measured using conventional means for centuries. Snow depth observations are performed at most weather stations in cold climates. Accurate snow mass information can be derived from surface observations of snow depth and SWE for regions and time periods with a sufficiently dense observing network (Brown and

Derksen 2013) but there remain vast alpine and high latitude regions with insufficient coverage by conventional observing networks (Brown et al. 2019). SWE is further measured in fixed point-wise locations using snow scales and microwave instruments. Ground-based snow measurements are severely limited by a lack of confidence in how they capture the variability in conditions across larger scales, particularly for heterogeneous landscapes. An improvement to point-wise observations are multiple *in situ* snow courses along a predefined transect. These are available from several national and regional agencies (Haberkorn 2019) and provide more representative estimates on a regional scale. The amount of snow course data is however even more limited in time and space; thus, they are more often used as reference data.

Regional to hemispheric estimation of SWE and snow mass has been obtained since the 1980s from standalone passive microwave observations (e.g. Chang et al. 1990; Kelly et al. 2003) or from synergistic approaches combining satellite observations with ground data (Pulliainen 2006; Takala et al. 2011, 2017). Standalone passive microwave approaches are somewhat limited in their applicability for hemispheric monitoring, but in combination with *in situ* data perform similar to reanalysis datasets (Mortimer et al. 2020). Both EO- and model-based approaches can be further improved using appropriate bias correction techniques (Pulliainen et al. 2020). A key challenge for satellite passive microwave instruments is their coarse spatial resolution, which prohibits their accurate utilization for mountainous regions. There is potential in C-band SAR to provide high-spatial-resolution snow depth information in mountainous areas (Lievens et al. 2019), but these estimates are still somewhat uncertain and only available with relevant coverage since 2014, thus limiting the potential to retrieve time series relevant for climate studies.

*h. Glaciers*

At decadal to annual time scales, glaciers act as storages with related changes, while at annual scales, their annual mass-turnover corresponds to hydrological fluxes. As such, glaciers contribute to runoff during dry/summer seasons even in years with positive annual mass-balances, i.e. annually net increase in storage (Weber et al. 2010; Huss 2011). Glaciers are among the highest-confidence natural indicators of climate change (GLIMS and NSIDC 2005; Paul et al. 2009; Bojinski et al. 2014; RGI 2017). Water storage in glaciers cannot be directly measured but is assessed from inventories of glacier surface area and glacier thickness estimates. Glacier inventories are compiled at national to regional levels mainly based on optical images from air and spaceborne sensors (Paul et al. 2009). Glacier ice thickness observations from field and airborne surveys (Gärtner-Roer et al. 2014; Welty et al. 2020) are used to calibrate analytical and numerical models to estimate the regional and global storage of glacier ice (Farinotti et al. 2019).

Glacier mass changes have been measured *in situ* with seasonal to annual resolution at a few hundred glaciers worldwide, with a few observation series reaching back to the early 20th century (Zemp et al. 2015). Decadal glacier elevation and volume changes are assessed from topographic surveys and differencing of related maps and digital elevation models (Zemp et al. 2015), using density assumptions (Huss 2013) for conversion to glacier mass changes. Such geodetic mass changes are available for several glaciers from terrestrial surveys back to the late 19th century, for several hundred glaciers from aerial and early space borne surveys back to the mid-20th century, and potentially for all glaciers from spaceborne surveys since the beginning of the 21st century (WGMS 2020; Zemp et al. 2019). For data-scarce regions, these results have been complemented with regional glacier change estimates based on satellite altimetry and gravimetry (Moholdt et al. 2012; Bolch et al. 2013; Treichler and Kääb 2016; Gardner et al. 2013; Wouters et al. 2019).

#### *i. Ice sheets*

Ice sheets are defined as ice volumes covering an area of continental size. Only the Antarctic and Greenland ice sheets comply with this definition, with Antarctica often subdivided into the West and East Antarctic ice sheets. By definition, ice sheets only concern the grounded part; the floating parts are attributed to the ice shelf, the melt of which does not change the sea level (Cogley et al. 2011).

The water stored in ice sheets is estimated from ice sheet volume measurements, which are derived by combining airborne radar measurements to define the bottom boundary of the ice and surface height measurements made by airborne and satellite laser and altimeters. Both Greenland and Antarctica have been almost completely covered in this way. Changes in ice mass can be determined in various ways: by elevation change measurements from satellite altimetry, combined with models of snow density and firn compaction; by estimating changes in mass flux across the grounding lines, using ice velocities from radar interferometry combined with meteorological observations and atmospheric reanalysis of interior precipitation, and climate-firn models; and most reliably by satellite gravity measurements of GRACE/GRACE-FO. Uncertainties in global isostatic adjustments is a major error source in mass change estimates, with uncertainties up to 30% in Antarctica and 5-10% in Greenland (Shepherd et al. 2018).

#### *j. Water stored in living biomass*

About 40–80% of the world's terrestrial vegetation is composed of water, but this fraction may strongly vary between species, seasons, and meteorological conditions (e.g. Yebra et al. 2018). The remaining fraction is referred to as living (dry) biomass, which can be divided into the two main components above-ground biomass (AGB) - including living stems, branches, leaves, and fruits - and below-ground biomass (BGB), commonly defined as living root biomass (Penman et al. 2003). The ratio below- and above-ground biomass (known as

root:shoot ratio) is between 0.2 and 0.4 for most forest ecosystems but may vary considerably across biomes and vegetation types, ranging from 0.1 in some forest types to 26 in a cool temperate grassland (Mokany et al. 2006).

While vegetation water content has frequently been estimated from optical remote sensing observations at the local scale (e.g. Dorigo et al. 2009), only very few studies attempted to estimate it for larger spatial domains (e.g. Yebra et al. 2018). On the other hand, microwave observations have a very high sensitivity to the water stored in above-ground vegetation (Jackson and Schmugge 1991). Datasets of microwave VOD, which describes the attenuation of microwave radiance by vegetation, have been developed for various sensors, even over multi-decadal timescales (e.g. Moesinger et al. 2020), and related to total vegetation water content (Konings and Momen 2018).

Alternatively, vegetation water content can potentially be estimated from EO-derived AGB and extended to total biomass (AGB+BGB) by applying a plant-specific root:shoot ratio. By applying a multiplication factor based on the characteristic plant-specific relative water content, the total biomass can be used to estimate the total water stored in the vegetation (Yebra et al. 2018). Both optical and radar data can be useful for biomass measurements, but commonly SAR and LIDAR data are used in combination (e.g. Asner et al. 2012; Mitchell et al. 2017). EO-based AGB estimates need ancillary data, e.g., ground data and close-range remote sensing sources such as terrestrial and airborne LIDAR data for the calibration and validation of the satellite observations (Herold et al. 2019).

Large uncertainties in global estimates of water stored in biomass result from various measurement errors and generalization throughout the computation chain and from the uneven distribution and quality of *in situ* data. Additionally, uncertainty information associated with the ground data is often not available. Current biomass mapping from space is hindered by its disconnection from plot-based national forest inventory efforts (Böttcher et

al. 2017), and varying definitions used for the source data, and methods used to construct the maps (Herold et al. 2019). Remote sensing signals can also saturate at high biomass values, making mapping in natural and tropical forests particularly uncertain (Avitabile et al. 2016).

### 3. Observing Water Cycle Fluxes

#### *a. Ocean evaporation*

With a share of 86% to total global evaporation, evaporation from the oceans dominates the surface-to-atmosphere flux of the water cycle. Direct measurements of ocean evaporation through the eddy-covariance method are currently limited to selected locations with limited duration due to technical challenges in operating the instruments from mobile platforms at sea (Edson et al. 1998; Landwehr et al. 2015). Evaporation cannot be directly observed from satellites because it does not emit, reflect, or absorb electromagnetic radiation. Evaporation is therefore commonly estimated by parameterizing ocean evaporation process models with surface meteorological variables that can be observed (Liu et al. 1979; Fairall et al. 2003). The required variables are SST, wind speed, near-surface air temperature, and humidity, which can be measured from in situ platforms, including Voluntary Observing Ships (VOS), research cruises, and moored buoys, or derived from optical and/or microwave satellites. VOS observations have a rich history before satellites became available (e.g. Josey et al. 1999). The VOS provide direct observations for all variables required to estimate the moisture flux at the ocean surface, but the observations are spatiotemporally inhomogeneous and clustered over the major shipping lanes. However, in densely sampled regions such as the North Atlantic, the VOS-based flux estimates with a multi-decade span are a valuable *in situ* climatology (Berry and Kent 2011).

Not all variables can be directly retrieved from satellites. SST and wind speed have a relatively direct relationship to the radiance measured by the satellites, whereas air

temperature and humidity have to be derived indirectly because the electromagnetic signal is emitted from relatively thick integrated atmospheric layers. Retrieval algorithms are fully empirical and require ancillary data from, e.g., ships and buoys. Presently, the accuracy of derived air temperature and humidity stands as the main source of uncertainty in satellite-based ocean flux products (e.g. Prytherch et al. 2015; Liman et al. 2018), but recent technological advances hold great promise in reducing the uncertainties input variables (e.g. Gentemann et al. 2020).

Reanalysis products have also been used to estimate ocean evaporation (directly related to latent heat flux), but their fidelities are affected by the uncertainties and coverage of the satellite observations assimilated (e.g. Yu et al. 2017; Robertson et al. 2020). Changes in ocean salinity (See sidebar) offer a proxy for inferring ocean evaporation in regions where evaporation dominates over precipitation such as subtropical high-salinity regimes (e.g. Yu et al. 2020). However, the contributions of ocean dynamics need to be accounted for.

#### *b. Land evaporation*

Corresponding to approximately two thirds of the precipitation falling over the continents, terrestrial evaporation is the second largest hydrological flux over land (Gimeno et al. 2010; Miralles et al. 2011). Its fast response to radiative forcing makes evaporation an early diagnostic of changes in climate, while its pivotal influence on land–atmosphere interactions leads to either amplification or dampening of weather extremes such as droughts or heatwaves (Miralles et al. 2019; Seneviratne et al. 2010).

Today, terrestrial evaporation remains one of the most uncertain and elusive components of the Earth’s water balance: it cannot be observed directly from space, and it is only seldom measured in the field through the eddy-covariance method, which often have limited spatial



representativeness, particularly over heterogeneous landscapes (Miralles et al. 2011; Fisher et al. 2017).

A range of datasets have been proposed that indirectly derive evaporation from models that combine satellite-observed environmental and climatic drivers of the flux (Fisher et al. 2017; McCabe et al. 2019; Jung et al. 2019). These datasets largely rely on multiple sensors from the Aqua and Terra platforms, and some long records also include data from earlier optical (e.g., AVHRR) and microwave (SSM/I, SMMR) sensors or use satellite soil moisture data in their retrievals (e.g. Martens et al. 2017). Several studies brought to light strong discrepancies amongst widely-used observation-based global land evaporation datasets (e.g. Talsma et al. 2018; Miralles et al. 2016; McCabe et al. 2016). Current global datasets share (i) systematic errors in semiarid regimes and tropical forests, (ii) an imperfect representation of water stress and canopy interception, and (iii) a poorly constrained partitioning of terrestrial evaporation into its different components (transpiration, interception loss, bare soil evaporation, snow sublimation, and open water evaporation). Few algorithms to compute transpiration include the effect of CO<sub>2</sub> fertilization processes on water use efficiency explicitly, which can be crucial to address long-term trends (Miralles et al. 2016). Nonetheless, these satellite-based datasets of land evaporation are still used as reference for a wide range of climatic applications, even though recent reanalysis datasets (such as ERA5) show clear improvements with respect to their predecessors (Martens et al. 2018).

### *c. Precipitation over ocean and land*

Precipitation, both liquid (rainfall) and frozen (snowfall), is spatially very inhomogeneous and can vary rapidly in places with mechanical lifting such as mountains or coastlines. There is also significant diurnal variability with the peak of land precipitation occurring in the late afternoon and early evening, posing high demands on the observation systems.

Precipitation over land is measured quite well by the dense networks of rain-gauges operated by many countries. The number of rain-gauges operated around the world is roughly 200,000 (Kidd et al. 2017), many of which have been used to produce global gridded products (Schneider et al. 2014; Harris et al. 2014). Rain-gauge measurements are influenced by systematic gauge measuring errors, mainly caused by wind-effects on precipitation, which is particularly large for snowfall. The interpolated gridded rain-gauge measurements have substantial uncertainty and sampling errors over complex terrain or in poorly sampled regions.

Several countries also operate operational radar networks, e.g., the US, Europe, and Japan (Zhang et al. 2016a; Makihara 1996; Huuskonen et al. 2014). Various attempts to homogenize existing networks have failed thus far, as they all have somewhat different objectives, quality control, and calibration procedures (Saltikoff et al. 2019). Besides, homogenization is hampered by the extremely large data volumes and limited areal coverage. The retrieval of precipitation from satellites remains challenging due to the strong intermittency and variability of precipitation in space and in time, as well as the fundamentally under-constrained nature of precipitation algorithms. Nonetheless, spaceborne radars and radiometers have successfully retrieved precipitation over land (Petersen et al. 2016; Hou et al. 2014) but their sampling remains poor, and accumulations have thus focused on “merged” products constructed with observations from multiple GEO and/or LEO satellites with or without gauge networks to compensate the drawbacks inherent to individual observations. Additionally, recent approaches for improving rainfall accumulations from space have considered the integration with satellite soil moisture products (Massari et al. 2020; Pellarin et al. 2020). Reanalysis datasets that integrate precipitation observations (e.g., ERA5, NCEP–NCAR) could in principle provide more accurate estimates than pure observation-based products but are equally affected by limitations in the coverage of ground

observations, inconsistencies between the assimilated datasets, and errors in numerical modelling (Tarek et al. 2020).

Despite being observationally constrained, the multitude of daily precipitation datasets based on rain gauge measurements, remote sensing, and/or reanalyses, have demonstrated a large disparity in the quasi- global land mean of daily precipitation intensity (e.g., (Herold et al. 2019). Masunaga et al. (2019) showed a contrast in global mean and extreme precipitation accumulations of satellite-in situ merged products, with stronger differences in their extreme precipitation. In general, Alexander et al. (2020) have shown that global observation-based precipitation products have potential for climate scale analyses of extreme precipitation frequency, duration and intensity. Specifically, reanalysis products tend to be much more variable than the observation-based products, particularly over the global oceans (Pellet et al. 2019).

Snowfall products are determined much like their rain counterparts but tend to have an added degree of difficulty associated with them. For radars, snow is less reflective than rain for the same size particles and since snowfall is often lighter than rainfall, echoes are generally much weaker. The GPM radar satellite is only able to detect moderate to heavy snowfall events. CloudSat, while more sensitive, is a nadir staring instrument which limits sampling to only climatological applications. Its W-band radar, while capable of better sampling, is still limited in its ability to uniquely convert echoes into meaningful snowfall rates given the great variability of particle sizes and densities. In mountainous regions, where snow tends to be most important, radar retrievals are further complicated by clutter from nearby mountains. The added complication for passive microwave retrievals is the relative lack of unique scattering signals over already snow-covered ground. The retrieval of orographic snowfall is challenging as this is typically characterized by copious snowfall with little or no deep cloud developments that are key to characterize precipitation events from

passive microwave and infrared observations (Shige and Kummerow 2016; Gonzalez et al. 2019).

#### *d. River discharge*

Regular measurements of river water height started long ago, and include well-known examples such as the annual minimum and maximum water levels of the Nile river for the years 622–1922 (Whitcher et al. 2002). Today, *in situ* systems still offer the most accurate basis for monitoring river discharge (Fekete et al. 2002). The majority of the river flux into the oceans (~70%) is covered by a set of 472 global gauging stations, of which 327 are freely available (Looser et al., 2007) but usually shared only with a substantial delay by the national authorities that control the observations. Consequently, the temporal coverage of the available data is heterogeneous, with the highest number of stations available for the period 1980-2000. Because of the incomplete coverage of observations, estimations of total river discharge into the oceans rely on statistical or model-based extrapolation methods (e.g. Baumgartner and Reichel 1975; Milliman and Farnsworth 2011; Ghiggi et al. 2019; ) .

Remote sensing provides a valuable additional source of flow data for unmonitored or infrequently monitored rivers. Discharge can be estimated using particle image velocimetry and bathymetric LIDAR, though uncertainties in depth, flow speed, and estimated volumetric flow rates can be large (Huang et al. 2018; Kinzel and Legleiter 2019). Satellite altimetry coupled with satellite imagery and hydrodynamic modelling also offer adequate solutions (Kittel 2020), but uncertainties are large for rivers substantially obscured by riparian forest cover or ice covers and ice jams in winter, causing a seasonal bias with increased uncertainties in the discharge estimates (Hicks and Beltraos 2008). Finally, short-lived flood flows in dryland rivers can be difficult to quantify using remote sensing methods.

#### *e. Groundwater recharge and discharge*

Recharge of groundwater occurs by percolating precipitation and surface water, while losses are due to discharge to continental surface water bodies and to the ocean, evaporation, and groundwater pumping. Groundwater storage typically responds in a delayed and smoothed way to precipitation dynamics while actual residence times of groundwater can vary over several orders of magnitude depending on the climate and hydrogeological conditions and on its depth below the Earth surface (Foster et al. 2013). Groundwater recharge occurs at widely varying rates, which can be modulated by human use of the landscape and land cover change. Groundwater recharge rates may be enhanced by managed aquifer recharge, which is widely-used globally and is estimated to contribute  $\sim 10 \text{ km}^3$  annually to the global groundwater system ( $\sim 1\%$  of total groundwater extraction) (Stefan and Ansems 2018; Dillon et al. 2019).

Groundwater discharge naturally occurs either as submarine groundwater discharge (SGD) or as groundwater discharge to rivers, lakes and springs. SGD can be divided in three components: groundwater discharge below sea level (fresh SGD), meteoric groundwater discharge above sea level near the coast (near-shore terrestrial groundwater discharge; NGD), and recirculated sea water (Luijendijk et al. 2020). Fresh SGD and NGD combined correspond to coastal groundwater discharge (CGD) (Luijendijk et al. 2020). Total SGD is difficult to quantify due to its spatial and temporal variability (Sadat-Noori et al. 2015; Srinivasamoorthy et al. 2019) and the difficulty to measure it. Available techniques are water budgets, hydrogeological modeling, physical measurements, and the use of geochemical tracers (Srinivasamoorthy et al. 2019). Contrary to river discharge, groundwater discharge is usually not monitored, and there is no global database of SGD data.

*f) Glacier and ice sheet annual turnover*

Annual glacier mass turnover can be measured at individual glaciers by the component or flux-divergence approach (Bamber and Rivera 2007). However, at regional to global scale corresponding estimates are only available from modelling studies (Kaser et al. 2010; Braithwaite and Hughes 2020; Huss and Hock 2015). The annual mass turnover can be estimated from the mass-balance amplitude, expressed by half the difference between winter and summer balances. The runoff from snow and glaciers in mountain regions feed rivers and groundwater, while some is evaporated (Goulden and Bales 2014). In the Arctic and Antarctic, glaciers often flow directly into the ocean and lose mass through meltwater discharge and calving of ice (King et al., 2020).

Similarly, the Greenland and Antarctic ice sheets feed large amounts of freshwater to the ocean (Enderlin et al. 2014; IPCC 2019). Although the fresh water supply from ice sheets to the ocean is large, observation gaps cause large uncertainties (IPCC 2019). Ice sheet fluxes to the oceans can be determined from satellite measurements of ice velocities and airborne radar thickness around the perimeter of the ice sheet, with major error source being the unknown depths of key outlet glacier systems, especially in East Antarctica. Freshwater flux estimates based on GRACE or elevation changes from space or airborne laser and radar measurements are similarly inaccurate due to errors in snowfall and firn compaction estimates, and the “steady state” ice sheet velocities. Prior to the satellite era (starting in 1992) the knowledge of ice sheet mass balance is highly uncertain and strongly dependent on model assumptions (Slater et al. 2020).

#### *g) Anthropogenic Water Use*

According to the review about the human impact of the global water cycle by (Abbott et al. 2019) the total human water appropriation is estimated to flux magnitude as large as a quarter of total land precipitation. Freshwater used for irrigation, livestock, and industrial and

domestic consumption is primarily extracted from groundwater and surface water bodies and flows (blue water). Irrigation accounts for approximately 70% of anthropogenic freshwater withdrawals worldwide (Foley et al. 2011; Shiklomanov 2000). Since 1958, global statistics on anthropogenic water use have been made available by FAO (FAO 2021). Data are reported by each country as annual volumes with a usual delay of 2-4 years, are globally incomplete, and lack standardization across different countries. Data are therefore of limited use for characterizing water use responses to climate variability at sufficient spatial scale and temporal resolution. Other national and sub-national surveys may be available (e.g. Deines et al. 2017), but not only are these datasets uncertain, they are also inadequate because they are spatially and temporally lumped.

Remote sensing has emerged as a promising means to provide spatially and temporally explicit estimates of irrigation water volumes, thus overcoming the above-mentioned limitations. Optical and thermal remote sensing have been used to estimate actual evaporation, which can be coupled to the water/energy balance allowing to estimate irrigation volumes (Droogers et al. 2010; van Dijk et al. 2018; Lopez et al. 2020). Because of its direct relationship with irrigation, soil moisture, globally observed from satellites, is naturally designed to inform about the amount of water entering the soil (Kumar et al. 2015; Brocca et al. 2018; Jalilvand et al. 2019; Zaussinger et al. 2019). However, the coarse spatial resolution (10 to 40 km) of most soil moisture products represents a major constraint for accurate irrigation retrieval.

Once irrigation volumes are estimated, it would be possible to determine groundwater abstraction rates (e.g. Lopez et al. 2020). Although gravimetry-based remote sensing can inform about changes in TWS globally (Voss et al. 2013; Famiglietti 2014), they do not differentiate between natural and anthropogenic loss, or between the different types of water use. Besides, they are not suited for the spatial scales required for water resource

management. For regional groundwater monitoring, multi-spectral and microwave remotely sensed data together with land surface hydrological models are therefore required. Current global estimates of agricultural water use are still purely model-based (Siebert and Döll 2010).

A detailed breakdown of anthropogenic water use in cities is not available globally, but case studies using an urban metabolism approach are available for a few cities (e.g. Sahely et al. 2003; Kenway et al. 2011). The best prospects for deriving urban-area specific data are from global modelling of integrated hydrological and water resources and demand at sufficient scale to resolve urban areas (e.g. Wada et al. 2014; Luck et al. 2015). Focus in these larger-scale models is on blue water use (water use related to irrigation, derived from groundwater, rivers, and lakes), but green (derived from natural precipitation and soil moisture) and grey water (water required to assimilate pollution) availability and use in cities is growing. New developments in urban climate modelling (Hamdi et al, 2020) and urban land surface characterization (WUADAPT 2020) at meso- to micro-scale promise much better characterization of the urban water/energy balance, including some urban climate models that explicitly address the new developments in sustainable urban water supply (e.g. Broadbent et al. 2019).

#### **4. Integrating Water Cycle Components at Various Scales**

The recent states and observed changes of the Earth's water storage compartments are summarized in Table 1 and Figure 1, while those of the annual fluxes are collected in Table 2 and Figure 2. Even at these coarse scales, uncertainties of many of the components are large. Integrating a multiplicity of water cycle datasets into a single consistent dataset representative of the entire water cycle can help to optimize existing water cycle products or identify deficiencies in current observations.



776 *a. Integration strategies*

777 Dataset integration requires careful choices regarding the individual products of a single  
778 variable, the combination strategy, and appropriate spatial and temporal resolutions and  
779 domains. All these choices control if and how water cycle closure and consistency is  
780 eventually achieved. Ideally, coherence between water cycle products is already enforced at  
781 the retrieval stage (Popp et al. 2020; Lawford et al. 2004) but this is generally impractical  
782 given the many expert groups working on different water cycle components. Thus, their  
783 coherence is generally assessed *a posteriori*, either:

- 784 • as a diagnostic of satellite product skill to quantify the sources of water imbalance and  
785 the uncertainties of each component (Sheffield et al. 2009; Moreira et al. 2019);
- 786 • to optimize the estimation of the components, using water budget closure as a  
787 constraint (Pan and Wood 2006; Munier et al. 2014);
- 788 • to estimate missing information in the water cycle, e.g., an unobserved component  
789 (Azarderakhsh et al. 2011; Hirschi and Seneviratne 2017; Pellet et al. 2020) or an  
790 available component at a coarse resolution that requires downscaling (Ning et al.  
791 2014).

792 The datasets can be combined in four ways:

- 793 • No optimization of the water components: Based on *a priori* knowledge on the quality  
794 of the data, single datasets of each water component are combined without modifying  
795 their values. This type of combination is used to study water cycle linkages or to  
796 diagnose the quality of the individual datasets (Sheffield et al. 2009; Moreira et al.  
797 2019; Rodell et al. 2004).
- 798 • Assimilation of the components into surface or hydrological models to ensure budget  
799 closure (Pan and Wood 2006; Pan et al. 2012; Sahoo et al. 2011; Zhang et al. 2018).

This is a non-trivial task as it requires appropriate *a priori* bias correction, uncertainty estimates, and observation operators. Besides, it may impose model structures and dynamics on the observed variability.

- Statistical optimization between the components to force water budget closure without the use of a model (Rodell et al. 2015; Pellet et al. 2019; Aires 2014), which also requires estimates of dataset bias and uncertainties.
- Including energy budget constraints (Thomas et al. 2020; Rodell et al. 2015; Stephens et al. 2012).

Since not all water cycle components can be sufficiently well observed, their integration always requires data that are not purely observational, e.g., water vapor divergence from reanalysis or discharge estimates of ungauged basins estimated from an observation-driven hydrologic model (Pellet et al. 2019).

#### *b. Water cycle integration across spatial and temporal scales*

Water cycle integration can be done over a large range of spatial and temporal domains (Appendix Table A3). The larger the scales, the lower the uncertainties of the individual inputs due to the averaging of errors, hence the easier it becomes to close the water budget. Rodell et al. (2015) made the first attempt to obtain globally consistent water and energy fluxes at a continental spatial resolution and for the climatological season, using satellite, *in situ*, and reanalysis data. The study highlighted the need for a snow measurement mission to better constrain the cold land hydrology as well as for a satellite mission dedicated to measuring evaporation to improve water budget closure over tropical areas. A water budget closure study performed over 341 basins around the world based on reanalysis and river discharge measurements raised the need of a mission dedicated to moisture convergence monitoring (Hirschi and Seneviratne 2017). Even if convergence estimates from reanalysis models are

still better than any P–E estimates (Trenberth and Fasullo 2013; Munier et al. 2018; Rodell et al. 2011; Trenberth et al. 2011)<sup>[OBJ]</sup> revealed that particularly over the tropics E is still too poorly simulated by land surface models (Sahoo et al. 2011; Munier et al. 2018; Rodell et al. 2011).

Regional water cycle integration studies have covered several parts of the world for various purposes but with mixed success. For South America, water budget integration has been used to estimate river discharge in several ungauged sub-basins of the Amazon river (Azarderakhsh et al. 2011) and to assess continental closure (Moreira et al. 2019). In Africa, it was used to assess the water balance of the Volta basin (Ferreira and Asiah 2016) and Lake Victoria (Swenson and Wahr 2009). Mariotti et al. (2002) studied the long-term trends in water cycle components of the Mediterranean and estimated water flow through the Gibraltar strait, which was later confirmed by a purely observation-based study (Pellet et al. 2019). Integrated water budget approaches were also used to quantify freshwater discharge from the entire pan-Arctic region (Syed et al. 2007; Landerer et al. 2010). For the US it was shown that water budget closure from remote sensing only was not possible because of large errors in the individual products (Sheffield et al. 2009; Gao et al. 2012). Over Canada, a comprehensive climatology of the joint water and energy budgets was developed for the Mackenzie (Szeto et al. 2008) and Saskatchewan (Szeto 2007) River basins and later extended to the entire country (Wang et al. 2014, 2015). Liu et al. (2018) used water cycle integration to assess the seasonal cycles and trends (1982–2011) of the water budget components over the Tibetan Plateau while Pellet et al. (2020) reconstructed long term (1980–2015) water storage change over the main river basins in Southeast Asia and showed the dominant contribution of precipitation in its interannual variability.

At the pixel level, Zhang et al. (2018) created a 25-year 0.5° resolution CDR at the global scale, using satellite observations, reanalysis data, and water cycle budget closure optimization. This CDR fits the need of a comprehensive database to describe the water cycle in a coherent

way, but still at a coarse spatio-temporal resolution and heavily relying on hydrological modelling.

*c. Example of Global Integration of state-of-the-art Fluxes*

Simple assessments at global and annual scales can be used to get a first grasp on the coherency between datasets. Here, we use a description of the terrestrial water cycle budget integrated over all continental surfaces, i.e., the change in TWS ( $dTWS$ ) = terrestrial precipitation ( $P_t$ ) – terrestrial evaporation ( $E$ ) – Discharge ( $R$ ).  $R$  includes both river ( $R_r$ ) and groundwater discharge ( $R_g$ ), which is difficult to estimate directly. But, when assuming that  $dTWS$  equals zero at the annual scale,  $R_g$  can be estimated from the state-of-the-art numbers reported in this study by:

$$R_g = dTWS + P_t - E_t - R_r = 0 + 123,300 - 69,200 - 39,981 = 14,119 \pm 9,004 \text{ } 10^3 \text{ km}^3 \text{ yr}^{-1}$$

The uncertainty estimate is derived by standard error propagation of uncorrelated gaussian-distributed errors. Despite the very large uncertainty range, it does not cover the state-of-the-art  $R_g$  estimate ( $0.5 \pm 0.3 \text{ } 10^3 \text{ km}^3 \text{ yr}^{-1}$ ; Table 2). Biases in the individual components directly translate into a biased discharge estimate, while it is difficult to attribute this imbalance to a specific dataset. Also, uncertainties in each product are crucial to weigh certain datasets over uncertain ones, and to estimate *a posteriori* the uncertainty of the final solution. While combining yearly data at the global scale reduces uncertainties thanks to the cancelling of errors, and the above representation may be too simplistic, e.g., assuming  $dTWS = 0$ , it does show that we are still far from perfect closure based on observations only, even at these coarse scales. This becomes increasingly challenging at finer spatial and temporal scales.

The water budget cannot be accurately closed if one of the components is not observed. This is even more so the case for the long-term trends (Table 1; Table 2). Global trend

estimates are still too uncertain for many components, because of too short observation records or failing intercalibration of sensors over time. Besides, closing trends in the water cycle components requires a sufficiently long common baseline period, which is currently lacking for the ECVs that do provide trends based on scientific consensus (Table 1; Table 2). Yet, various studies assessed trends and their underlying drivers in multiple observations of individual ECVs, often in combination with trends in reanalysis products, e.g., for precipitation (Zhang et al. 2007), soil moisture (Preimesberger et al. 2020), land evaporation (Zhang et al. 2016b), and runoff (Yang et al. 2019). Several recent studies demonstrated consistency in trends between a selection of water cycle ECVs, mostly between continental ice melt and sea level rise (Zemp et al. 2019; Shepherd et al. 2020; Raj et al. 2020), but substantial uncertainty remains for the land water storage components (Cazenave et al. 2018).

## 5. Synthesis and outlook

Long-term monitoring the Earth's water cycle has made great progress in recent decades, but many observational gaps still need to be overcome to fully characterize variability in individual components and allow for a comprehensive and consistent assessment of the water cycle as a whole. Table 3 and 4 summarize the main challenges per water cycle component (status and long-term changes (trends) of both, the changes in storage but also changes in fluxes as available) confronted with the foreseen observational and methodological developments. Several challenges shared by multiple water cycle components are summarized in the following.

### *a. Continuation and expansion of existing observation systems*

If at all, trends in water cycle components can only be observed with great uncertainty, which is mainly due to insufficient length and homogeneity of the observations. Thus, it is of utmost performance to restore historical satellite and ground data, continue existing

measurement concepts and harmonize past, current and future observing systems. Even satellite observing systems with demonstrated skill for a range of variables (e.g., L-band radiometer observations for soil moisture and vegetation water, gravity observations for groundwater, ice sheets, and glaciers) have an uncertain future. The joint CEOS/CGMS working group Climate supports a strategic planning beyond the lifetime of a single mission. EUMETSAT's Satellite Application Facilities or the EU- Copernicus programs are already in line with this paradigm shift.

A major difficulty is the intercalibration of satellite datasets with varying quality and temporal/spatial characteristics over time. Yet, as shown by this review, satellites alone cannot solve for the entire balance and coordinated ground monitoring capacities are needed. Extensive networks of long-term fiducial *in situ* monitoring networks are fundamental in this respect, e.g., those federated within the Global Terrestrial Network for Hydrology (GTN-H), the Global Ocean Observing System (GOOS), and the Global Atmosphere Watch (GAW). However, their ambition to collect trustworthy observations worldwide is encumbered by lacking open data policies and the fact that many ground observing networks heavily rely on scientific project funding, causing observational gaps particularly in the global south. Support and advocacy for the national hydrological and meteorological services as well as space agencies to fund, collect, and make available these data must be expanded.

#### *b. New observation systems*

Several dedicated scientific satellite missions have been scheduled to fill existing gaps in water cycle observations, among them SWOT (Morrow et al. 2019), scheduled for launch in 2021. SWOT is expected to revolutionize continental water cycle observability, by allowing the global characterization of lake and river discharge dynamics in regions with sparse ground monitoring or restrictive data sharing policies. Apart from the Sentinel satellites

currently in orbit or already scheduled for launch, the EU-Copernicus program has defined several High Priority Candidate missions, of which CIMR, CRISTAL and ROSE-L have particular relevance for improved characterization of various water cycle components, including snow, ice sheets and shelves, glaciers, and soil moisture. In addition, new EO observation capabilities need to be developed for ECVs that thus far are hardly characterized, e.g., ground ice, anthropogenic water use, and groundwater recharge and discharge. Yet, by nature, these components will heavily rely on ground observations and consequently adequate ground infrastructure needs to be established, improved, and sustainably supported. In addition, artificial intelligence and machine learning should become routinely applied for reduction of retrieval errors and uncertainties of upcoming and existing missions.

*c. Integration of ECVs with other components and models*

In general, the integration of existing sensors (*in situ*, remote sensing) and techniques will close observational gaps. A new ECV total terrestrial water storage (TWS) would provide more timely and integrative data to directly close the continental water budget of P, E, R and dTWS (see Section 4). A long-term perspective for gravity observations from space is thus crucial.

But, no matter how sophisticated the satellites or observing systems are, observation errors in the individual products will always be present and lead to inconsistencies between ECVs, hampering a comprehensive assessment of the water cycle. Statistical integration methods can force consistency between ECVs and optimize individual components, but require estimates of their uncertainties, which are not trivial to obtain. Also data integration methods can profit from artificial intelligence and machine learning to reduce uncertainties and biases (Aires 2018). For instance, Beck et al. (2021) used ancillary data of surface properties in a Random Forest machine learning framework to explain errors at the pixel level

while closing the water budget. Such an approach can be trained at basins where sufficient (most importantly discharge) data are available to close the water budget and then applied to each location or pixel for which this requirement is not fulfilled. Structural errors (biases) can be state-dependent (e.g., for anthropogenic water use or discharge), have spatial or seasonal patterns, and directly translate into an imbalance in the water budget. Higher spatial and temporal resolutions may reveal important local climate signals, e.g., on extreme events, but closing the water budget at these scales becomes increasingly challenging. State-of-the-art closure methods analyze regions at the sub-basin scale, requiring knowledge of the inter-dependency of the sub-basins and the lateral (sub-) surface transport (Azarderakhsh et al. 2011; Pellet et al. 2020). This interdependency of sub-basins can be pushed even further to the pixel-scale but the spatial resolution of some datasets (e.g., GRACE) is a major limitation. However, integrating the datasets and imposing the budget closure can actually be a technical solution to downscale coarse resolution datasets, both spatially and temporally (Ning et al. 2014).

Improving model-data synthesis capabilities and reducing the spread of reanalysis products on precipitation, evaporation, and discharge is needed for an advanced closure of the water cycle, in particular at regional to local scales. This can be achieved by consolidating forcing data and auxiliary datasets, e.g., by using a common land-sea mask (Popp et al. 2020) or by constraining reanalyses with observations, e.g., satellite-observed ocean salinity (Yu et al. 2017).

This especially applies to the uncertainty of atmospheric moisture transport, which cannot be measured directly and is mostly inferred from reanalysis. Different approaches to model key elements (e.g., terrestrial interception loss) explain for some ECVs the lack of global closure in the water cycle. It is also concluded that integrated modelling approaches provide



the best prospect for resolving anthropogenic water use at the necessary scale and temporal resolution, with accounting and satellite data used for input and validation.

*d. Final remarks*

Available and clean water resources are one of our biggest challenges globally and are under pressure due to global change (UNESCO 2020). This requires consistent monitoring and long-term observation strategies. Water is a connecting element, but it is also the focus of various competing interests that can lead to serious political conflicts. While observational needs are currently expressed by the individual communities, the definition of future observation systems should consider following a more holistic approach and observe water cycle components as part of their global cycle and assess its variability in conjunction with the energy and carbon cycles. This should be adopted and implemented by high level organizations like GCOS, but also by the agendas of the WMO member states as well as of the WMO research agenda.

*Acknowledgments*

WD acknowledges ESA's QA4EO (ISMN) and CCI Soil Moisture projects. WD, CRV, AG, and KL acknowledge the G3P project, which has received funding from the European Union's Horizon 2020 research and innovation programme under grant agreement n° 870353. MIH and MS acknowledge ESA's CCI Water Vapour project. MS and RH acknowledges the support by the EUMETSAT member states through CM SAF. DGM acknowledges support from the European Research Council (ERC) under grant agreement no. 715254 (DRY-2-DRY).

We thank Gabi Hegerl and Robert Reinecke for their advice on the manuscript and  
Andrea Wessler for graphic editing. Finally, we thank the three anonymous reviewers for  
their very valuable suggestions for improvement and Peter Blanken for his editing.

#### *Data Availability Statement*

No data are used in this study.

## APPENDIX

Tables A1-A3 here

## Acronyms used in this study

Acronym	Full Spelling
Aeolus	ESA Satellite mission
AGB	Above-ground biomass
AMRS-2	Advanced Microwave Scanning Radiometer 2
ASCAT	Advanced Scatterometer
AVHRR	Advanced Very High Resolution Radiometer
BGB	below-ground biomass
C3S	Copernicus Climate Change Service
CDR	Climate Data Record
CGD	Coastal groundwater discharge
CIMR	Copernicus Imaging Microwave Radiometer
CRISTAL	Copernicus Polar Ice and Snow Topography Altimeter
dS	Total terrestrial storage change
E	Evaporation
ECV	Essential Climate Variable
EOS	Earth Observing System
ESA	European Space Agency
ESA CCI	ESA Climate Change Initiative
CryoVEx	CryoSat2 Validation Experiment
ET	Evapotranspiration
EUMETSAT	European Organization for the Exploitation of Meteorological Satellites
FAO	Food and Agriculture Organization
FTIR	Fourier-Transform-Infrared-Spektrometer
GAW	Global Atmosphere Watch
GCOS	Global Climate Observing System
GDL	groundwater discharge to lakes
GEO	Geostationary Orbit
GGMN	Global Groundwater Monitoring Network
GMSL	Global Mean Sea Level
GOOS	Global Ocean Observing System
GPCC	Global Precipitation Climatology Centre
GPM	Global Precipitation Measurement Satellite
GPS	Global Positioning System
GRACE	Gravity Recovery and Climate Experiment
GRACE-FO	GRACE Follow-On
GRDC	Global Runoff Data Centre
GRUN	global gridded runoff data
GTN-G	Global Terrestrial Network for Glaciers
GTN-H	Global Terrestrial Network for Hydrology
GTN-P	Global Terrestrial Network for Permafrost
GTN-R	Global Terrestrial Network for Rivers
ICESat	Ice, Cloud and land Elevation Satellite
ICWRGC	International Centre for Water Resources and Global Change
InSAR	Interferometry of Synthetic Aperture Radar
IPCC	Intergovernmental Panel on Climate Change

JAXA	Japan Aerospace Exploration Agency
LEO	Low Earth Orbit
LIDAR	Light Detection and Ranging
MERRA-2	Modern-Era Retrospective analysis for Research and Applications
MetOP	Meteorological Operational Satellite
MRMS	Sensor Radar Multi
NGD	Near-shore terrestrial groundwater discharge
JPSS	Joint Polar Satellite System
NSIDC	National Snow and Ice Data Center
P	Precipitation
R	All discharge
RACMO	Regional Atmospheric Climate Model
Rg	Groundwater discharge
rH	Relative humidity
root:shoot	ratio below- and above-ground biomass
ROSE-L	L-band Synthetic Aperture Radar)
Rr	River discharge
SAR	Synthetic Aperture Radar
SGD	Submarine groundwater discharge
SMAP	Soil moisture active passive
SMMR	Scanning Multichannel Microwave Radiometer
SMOS	Soil Moisture and Ocean Salinity
SROCC	Special Report on the Ocean and Cryosphere in a Changing Climate
SSM/I	Special Sensor Microwave / Imager
SST	Sea surface temperature
SWE	snow water equivalent
SWOT	Surface Water Ocean Topography
TCWV	Total column water vapor
TIRS	Thermal infrared sensors
TPW	Total Precipitable Water
TRMM	Tropical Rainfall Measuring Mission
TWS	Total terrestrial water storage
UN	United Nations
UNFCCC	United Nations Framework Convention on Climate Change
VOD	Vegetation optical depth

1002

## REFERENCES

- Abbott, B. W., and Coauthors, 2019: Human domination of the global water cycle absent from depictions and perceptions. *Nat. Geosci.*, **12**, 533–540, <https://doi.org/10.1038/s41561-019-0374-y>.
- Abolafia-Rosenzweig, R., M. Pan, J. L. Zeng, and B. Livneh, 2021: Remotely sensed ensembles of the terrestrial water budget over major global river basins: An assessment of three closure techniques. *Remote Sens. Environ.*, **252**, 112191, <https://doi.org/10.1016/j.rse.2020.112191>.
- Aires, F., 2014: Combining Datasets of Satellite-Retrieved Products. Part I: Methodology and Water Budget Closure. *J. Hydrometeorol.*, **15**, 1677–1691, <https://doi.org/10.1175/jhm-d-13-0148.1>.
- , 2018: Atmospheric Water Vapour Profiling over Ocean/Land and for Clear/Cloudy Situations Using Microwave Observations. Springer, Cham, 215–255.
- Albergel, C., and Coauthors, 2013: Skill and global trend analysis of soil moisture from reanalyses and microwave remote sensing. *J. Hydrometeorol.*, **14**, 1259–1277, <https://doi.org/10.1175/JHM-D-12-0161.1>.
- Allan, R. P., and Coauthors, 2020: Advances in understanding large-scale responses of the water cycle to climate change. *Ann. N. Y. Acad. Sci.*, **1472**, 49–75, <https://doi.org/10.1111/nyas.14337>.
- Asner, G. P., and Coauthors, 2012: High-resolution mapping of forest carbon stocks in the Colombian Amazon. *Biogeosciences*, **9**, 2683–2696, <https://doi.org/10.5194/bg-9-2683-2012>.
- Avitabile, V., and Coauthors, 2016: An integrated pan-tropical biomass map using multiple reference datasets. *Glob. Chang. Biol.*, **22**, 1406–1420,

- 1027 <https://doi.org/10.1111/gcb.13139>.
- 1028 Azarderakhsh, M., W. B. Rossow, F. Papa, H. Norouzi, and R. Khanbilvardi, 2011:
- 1029 Diagnosing water variations within the Amazon basin using satellite data. *J. Geophys.*
- 1030 *Res. Atmos.*, **116**, <https://doi.org/10.1029/2011JD015997>.
- 1031 Babaeian, E., M. Sadeghi, S. B. Jones, C. Montzka, H. Vereecken, and M. Tuller, 2019:
- 1032 Ground, Proximal, and Satellite Remote Sensing of Soil Moisture. *Rev. Geophys.*, **57**,
- 1033 530–616, <https://doi.org/10.1029/2018RG000618>.
- 1034 Bamber, J. L., and A. Rivera, 2007: A review of remote sensing methods for glacier mass
- 1035 balance determination. *Glob. Planet. Change*, **59**, 138–148,
- 1036 <https://doi.org/10.1016/j.gloplacha.2006.11.031>.
- 1037 Baumgartner, A., and E. Reichel, 1975: Die Weltwasserbilanz: Niederschlag, Verdunstung
- 1038 und Abfluß über Land und Meer sowie auf der Erde im Jahresdurchschnitt. Mit 19
- 1039 Tabellen sowie.
- 1040 Beck, H. E., and Coauthors, 2021: Evaluation of 18 satellite- And model-based soil moisture
- 1041 products using in situ measurements from 826 sensors. *Hydrol. Earth Syst. Sci.*, **25**, 17–
- 1042 40, <https://doi.org/10.5194/hess-25-17-2021>.
- 1043 Berg, A., and J. Sheffield, 2019: Evapotranspiration partitioning in CMIP5 models:
- 1044 Uncertainties and future projections. *J. Clim.*, **32**, 2653–2671,
- 1045 <https://doi.org/10.1175/JCLI-D-18-0583.1>.
- 1046 Berghuijs, W. R., R. A. Woods, and M. Hrachowitz, 2014: A precipitation shift from snow
- 1047 towards rain leads to a decrease in streamflow. *Nat. Clim. Chang.*, **4**, 583–586,
- 1048 <https://doi.org/10.1038/nclimate2246>.
- 1049 Berry, D. I., and E. C. Kent, 2011: Air-Sea fluxes from ICOADS: the construction of a new
- 1050 gridded dataset with uncertainty estimates. *Int. J. Climatol.*, **31**, 987–1001,

1051 <https://doi.org/10.1002/joc.2059>.

1052 Bindoff, N. L., and Coauthors, 2013: Chapter 10 - Detection and attribution of climate  
1053 change: From global to regional.

1054 Blazquez, A., B. Meyssignac, J. M. Lemoine, E. Berthier, A. Ribes, and A. Cazenave, 2018:  
1055 Exploring the uncertainty in GRACE estimates of the mass redistributions at the Earth  
1056 surface: Implications for the global water and sea level budgets. *Geophys. J. Int.*, **215**,  
1057 415–430, <https://doi.org/10.1093/gji/ggy293>.

1058 Bojinski, S., M. Verstraete, T. C. Peterson, C. Richter, A. Simmons, and M. Zemp, 2014: The  
1059 concept of essential climate variables in support of climate research, applications, and  
1060 policy. *Bull. Am. Meteorol. Soc.*, **95**, 1431–1443, [https://doi.org/10.1175/BAMS-D-13-](https://doi.org/10.1175/BAMS-D-13-00047.1)  
1061 00047.1.

1062 Bolch, T., L. Sandberg Sørensen, S. B. Simonsen, N. Mölg, H. Machguth, P. Rastner, and F.  
1063 Paul, 2013: Mass loss of Greenland’s glaciers and ice caps 2003–2008 revealed from  
1064 ICESat laser altimetry data. *Geophys. Res. Lett.*, **40**, 875–881,  
1065 <https://doi.org/10.1002/grl.50270>.

1066 Bonfils, C. J. W., B. D. Santer, J. C. Fyfe, K. Marvel, T. J. Phillips, and S. R. H. Zimmerman,  
1067 2020: Human influence on joint changes in temperature, rainfall and continental aridity.  
1068 *Nat. Clim. Chang.*, 1–6, <https://doi.org/10.1038/s41558-020-0821-1>.

1069 Bosilovich, M. G., F. R. Robertson, L. Takacs, A. Molod, and D. Mocko, 2017: Atmospheric  
1070 water balance and variability in the MERRA-2 reanalysis. *J. Clim.*, **30**, 1177–1196,  
1071 <https://doi.org/10.1175/JCLI-D-16-0338.1>.

1072 Böttcher, H., and Coauthors, 2017: *Independent Monitoring: Building trust and consensus*  
1073 *around GHG data for increased accountability of mitigation in the land use sector*.

1074 Braithwaite, R. J., and P. D. Hughes, 2020: Regional Geography of Glacier Mass Balance

1075        Variability Over Seven Decades 1946–2015. *Front. Earth Sci.*, **8**, 302,  
1076        <https://doi.org/10.3389/feart.2020.00302>.

1077    Brenninkmeijer, C. A. M., and Coauthors, 2007: Civil Aircraft for the regular investigation of  
1078        the atmosphere based on an instrumented container: The new CARIBIC system. *Atmos.*  
1079        *Chem. Phys.*, **7**, 4953–4976, <https://doi.org/10.5194/acp-7-4953-2007>.

1080    Broadbent, A. M., A. M. Coutts, K. A. Nice, M. Demuzere, E. S. Krayenhoff, N. J. Tapper,  
1081        and H. Wouters, 2019: The Air-temperature Response to Green/blue-infrastructure  
1082        Evaluation Tool (TARGET v1.0): an efficient and user-friendly model of city cooling.  
1083        *Geosci. Model Dev.*, **12**, 785–803, <https://doi.org/10.5194/gmd-12-785-2019>.

1084    Brocca, L., A. Tarpanelli, P. Filippucci, W. Dorigo, F. Zaussinger, A. Gruber, and D.  
1085        Fernández-Prieto, 2018: How much water is used for irrigation? A new approach  
1086        exploiting coarse resolution satellite soil moisture products. *Int. J. Appl. Earth Obs.*  
1087        *Geoinf.*, **73**, 752–766, <https://doi.org/10.1016/j.jag.2018.08.023>.

1088    Brown, J., O. Ferrians, J. Heginbottom, and E. Melnikov, 2002: Circum-Arctic Map of  
1089        Permafrost and Ground-Ice Conditions, Version 2 (Boulder, CO: National Snow and Ice  
1090        Data Center).

1091    Brown, R. D., and C. Derksen, 2013: Is Eurasian October snow cover extent increasing?  
1092        *Environ. Res. Lett.*, **8**, <https://doi.org/10.1088/1748-9326/8/2/024006>.

1093    ———, B. Fang, and L. Mudryk, 2019: Update of Canadian Historical Snow Survey Data and  
1094        Analysis of Snow Water Equivalent Trends, 1967–2016. *Atmos. - Ocean*, **57**, 149–156,  
1095        <https://doi.org/10.1080/07055900.2019.1598843>.

1096    Burnett, W. C., M. Taniguchi, and J. Oberdorfer, 2001: Measurement and significance of the  
1097        direct discharge of groundwater into the coastal zone. *Journal of Sea Research*, Vol. 46  
1098        of, Elsevier, 109–116.



- 1099 Busker, T., A. de Roo, E. Gelati, C. Schwatke, M. Adamovic, B. Bisselink, J.-F. Pekel, and  
 1100 A. Cottam, 2019: A global lake and reservoir volume analysis using a surface water  
 1101 dataset and satellite altimetry. *Hydrol. Earth Syst. Sci.*, **23**, 669–690,  
 1102 <https://doi.org/10.5194/hess-23-669-2019>.
- 1103 Byrne, M. P., and P. A. O’Gorman, 2016: Understanding decreases in land relative humidity  
 1104 with global warming: Conceptual model and GCM simulations. *J. Clim.*, **29**, 9045–  
 1105 9061, <https://doi.org/10.1175/JCLI-D-16-0351.1>.
- 1106 ———, and P. A. O’Gorman, 2018: Trends in continental temperature and humidity directly  
 1107 linked to ocean warming. *Proc. Natl. Acad. Sci. U. S. A.*, **115**, 4863–4868,  
 1108 <https://doi.org/10.1073/pnas.1722312115>.
- 1109 Cazenave, A., and Coauthors, 2018: Global sea-level budget 1993-present. *Earth Syst. Sci.*  
 1110 *Data*, **10**, 1551–1590, <https://doi.org/10.5194/essd-10-1551-2018>.
- 1111 Chang, A. T., J. L. Foster, and D. K. Hall, 1990: Satellite sensor estimates of northern  
 1112 hemisphere snow volume. *Int. J. Remote Sens.*, **11**, 167–171,  
 1113 <https://doi.org/10.1080/01431169008955009>.
- 1114 Chen, B., and Z. Liu, 2016: Global water vapor variability and trend from the latest 36 year  
 1115 (1979 to 2014) data of ECMWF and NCEP reanalyses, radiosonde, GPS, and  
 1116 microwave satellite. *J. Geophys. Res. Atmos.*, **121**, 11,442–11,462,  
 1117 <https://doi.org/10.1002/2016JD024917>.
- 1118 Chen, J., J. S. Famiglietti, B. R. Scanlon, and M. Rodell, 2016: *Groundwater Storage*  
 1119 *Changes: Present Status from GRACE Observations*.
- 1120 Cogley, J., and Coauthors, 2011: Glossary of glacier mass balance and related terms.  
 1121 <https://doi.org/10.5167/uzh-53475>.
- 1122 Cook, B. I., J. S. Mankin, K. Marvel, A. P. Williams, J. E. Smerdon, and K. J. Anchukaitis,

1123 2020a: Twenty-First Century Drought Projections in the CMIP6 Forcing Scenarios.  
 1124 *Earth's Futur.*, **8**, <https://doi.org/10.1029/2019EF001461>.

1125 ———, S. S. McDermid, M. J. Puma, A. P. Williams, R. Seager, M. Kelley, L. Nazarenko, and  
 1126 I. Aleinov, 2020b: Divergent Regional Climate Consequences of Maintaining Current  
 1127 Irrigation Rates in the 21st Century. *J. Geophys. Res. Atmos.*, **125**,  
 1128 <https://doi.org/10.1029/2019JD031814>.

1129 Crétaux, J. F., R. Abarca-del-Río, M. Bergé-Nguyen, A. Arsen, V. Drolon, G. Clos, and P.  
 1130 Maisongrande, 2016: Lake Volume Monitoring from Space. *Surv. Geophys.*, **37**, 269–  
 1131 305, <https://doi.org/10.1007/s10712-016-9362-6>.

1132 Deines, J. M., A. D. Kendall, and D. W. Hyndman, 2017: Annual Irrigation Dynamics in the  
 1133 U.S. Northern High Plains Derived from Landsat Satellite Data. *Geophys. Res. Lett.*, **44**,  
 1134 9350–9360, <https://doi.org/10.1002/2017GL074071>.

1135 van Dijk, A. I. J. M., J. Schellekens, M. Yebra, H. E. Beck, L. J. Renzullo, A. Weerts, and G.  
 1136 Donchyts, 2018: Global 5 km resolution estimates of secondary evaporation including  
 1137 irrigation through satellite data assimilation. *Hydrol. Earth Syst. Sci.*, **22**, 4959–4980,  
 1138 <https://doi.org/10.5194/hess-22-4959-2018>.

1139 Dillon, P., and Coauthors, 2019: Sixty years of global progress in managed aquifer recharge.  
 1140 *Hydrogeol. J.*, **27**, 1–30, <https://doi.org/10.1007/s10040-018-1841-z>.

1141 Dorigo, W. A., R. Richter, F. Baret, R. Bamler, and W. Wagner, 2009: Enhanced Automated  
 1142 Canopy Characterization from Hyperspectral Data by a Novel Two Step Radiative  
 1143 Transfer Model Inversion Approach. *Remote Sens.*, **1**, 1139–1170,  
 1144 <https://doi.org/10.3390/rs1041139>.

1145 ———, K. Scipal, R. M. Parinussa, Y. Y. Liu, W. Wagner, R. A. M. de Jeu, and V. Naeimi,  
 1146 2010: Error characterisation of global active and passive microwave soil moisture

1147 datasets. *Hydrol. Earth Syst. Sci.*, **14**, 2605–2616, <https://doi.org/10.5194/hess-14-2605->  
1148 2010.

1149 ———, and Coauthors, 2013: Global Automated Quality Control of In Situ Soil Moisture Data  
1150 from the International Soil Moisture Network. *Vadose Zo. J.*, **12**, vzj2012.0097,  
1151 <https://doi.org/10.2136/vzj2012.0097>.

1152 ———, and Coauthors, 2017: ESA CCI Soil Moisture for improved Earth system  
1153 understanding: State-of-the art and future directions. *Remote Sens. Environ.*, **203**, 185–  
1154 215, <https://doi.org/10.1016/j.rse.2017.07.001>.

1155 ———, I. Himmelbauer, L. Zappa, W. Preimesberger, D. Aberer, L. Schremmer, and I.  
1156 Petrakovic, 2021: The International Soil Moisture Network: serving Earth systems science  
1157 for over a decade. *Hydrol. Earth Syst. Sci*, *prep.*.

1158 Doughty, C. E., S. R. Loarie, and C. B. Field, 2012: Theoretical impact of changing albedo  
1159 on precipitation at the southernmost boundary of the ITCZ in South America. *Earth*  
1160 *Interact.*, **16**, 1–14, <https://doi.org/10.1175/2012EI422.1>.

1161 Downing, J. A., and Coauthors, 2006: The global abundance and size distribution of lakes,  
1162 ponds, and impoundments. *Limnol. Oceanogr.*, **51**, 2388–2397,  
1163 <https://doi.org/10.4319/lo.2006.51.5.2388>.

1164 Droogers, P., W. W. Immerzeel, and I. J. Lorite, 2010: Estimating actual irrigation  
1165 application by remotely sensed evapotranspiration observations. *Agric. Water Manag.*,  
1166 **97**, 1351–1359, <https://doi.org/10.1016/j.agwat.2010.03.017>.

1167 Durack, P. J., and S. E. Wijffels, 2010: Fifty-Year trends in global ocean salinities and their  
1168 relationship to broad-scale warming. *J. Clim.*, **23**, 4342–4362,  
1169 <https://doi.org/10.1175/2010JCLI3377.1>.

1170 ———, ———, and R. J. Matear, 2012: Ocean salinities reveal strong global water cycle

1171 intensification during 1950 to 2000. *Science* (80-. ), **336**, 455–458,  
 1172 <https://doi.org/10.1126/science.1212222>.

1173 Dwyer, J. G., and P. A. O’Gorman, 2017: Changing duration and spatial extent of midlatitude  
 1174 precipitation extremes across different climates. *Geophys. Res. Lett.*, **44**, 5863–5871,  
 1175 <https://doi.org/10.1002/2017GL072855>.

1176 Eakins, B. W., and G.F. Sharman, 2010: Volumes of the World’s Oceans from ETOPO1.  
 1177 *NOAA Natl. Geophys. Data Cent.*,  
 1178 [https://www.ngdc.noaa.gov/mgg/global/etopo1\\_ocean\\_volumes.html](https://www.ngdc.noaa.gov/mgg/global/etopo1_ocean_volumes.html) (Accessed August  
 1179 25, 2020).

1180 Edson, J. B., A. A. Hinton, K. E. Prada, J. E. Hare, and C. W. Fairall, 1998: Direct covariance  
 1181 flux estimates from mobile platforms at sea. *J. Atmos. Ocean. Technol.*, **15**, 547–562,  
 1182 [https://doi.org/10.1175/1520-0426\(1998\)015<0547:DCFEFM>2.0.CO;2](https://doi.org/10.1175/1520-0426(1998)015<0547:DCFEFM>2.0.CO;2).

1183 Eekhout, J. P. C., J. E. Hunink, W. Terink, and J. de Vente, 2018: Why increased extreme  
 1184 precipitation under climate change negatively affects water security. *Hydrol. Earth Syst.*  
 1185 *Sci.*, **22**, 5935–5946, <https://doi.org/10.5194/hess-22-5935-2018>.

1186 Elliott, G. W., 1974: Precipitation Signatures in Sea-Surface-Layer Conditions During  
 1187 BOMEX. *J. Phys. Oceanogr.*, **4**, 498–501, [https://doi.org/10.1175/1520-](https://doi.org/10.1175/1520-0485(1974)004<0498:psissl>2.0.co;2)  
 1188 [0485\(1974\)004<0498:psissl>2.0.co;2](https://doi.org/10.1175/1520-0485(1974)004<0498:psissl>2.0.co;2).

1189 Ellison, D., and Coauthors, 2017: Trees, forests and water: Cool insights for a hot world.  
 1190 *Glob. Environ. Chang.*, **43**, 51–61, <https://doi.org/10.1016/j.gloenvcha.2017.01.002>.

1191 Enderlin, E. M., I. M. Howat, S. Jeong, M. J. Noh, J. H. Van Angelen, and M. R. Van Den  
 1192 Broeke, 2014: An improved mass budget for the Greenland ice sheet. *Geophys. Res.*  
 1193 *Lett.*, **41**, 866–872, <https://doi.org/10.1002/2013GL059010>.

1194 van der Ent, R. J., and O. A. Tuinenburg, 2017: The residence time of water in the

1195 atmosphere revisited. *Hydrol. Earth Syst. Sci.*, **21**, 779–790,  
 1196 <https://doi.org/10.5194/hess-21-779-2017>.

1197 Entekhabi, D., and Coauthors, 2010: The soil moisture active passive (SMAP) mission. *Proc.*  
 1198 *IEEE*, **98**, 704–716, <https://doi.org/10.1109/JPROC.2010.2043918>.

1199 Fairall, C. W., and Coauthors, 2003: Bulk Parameterization of Air–Sea Fluxes: Updates and  
 1200 Verification for the COARE Algorithm. [http://dx.doi.org/10.1175/1520-](http://dx.doi.org/10.1175/1520-0442(2003)016<0571:BPOASF>2.0.CO;2)  
 1201 [0442\(2003\)016<0571:BPOASF>2.0.CO;2](http://dx.doi.org/10.1175/1520-0442(2003)016<0571:BPOASF>2.0.CO;2), [https://doi.org/10.1175/1520-](https://doi.org/10.1175/1520-0442(2003)016<0571:BPOASF>2.0.CO;2)  
 1202 [0442\(2003\)016<0571:BPOASF>2.0.CO;2](https://doi.org/10.1175/1520-0442(2003)016<0571:BPOASF>2.0.CO;2).

1203 Famiglietti, J. S., 2014: The global groundwater crisis. *Nat. Clim. Chang.*, **4**, 945–948,  
 1204 <https://doi.org/10.1038/nclimate2425>.

1205 FAO, 2021: AQUASTAT Database.  
 1206 <http://www.fao.org/nr/water/aquastat/data/query/index.html?lang=en>.

1207 Farinotti, D., M. Huss, J. J. Fürst, J. Landmann, H. Machguth, F. Maussion, and A. Pandit,  
 1208 2019: A consensus estimate for the ice thickness distribution of all glaciers on Earth.  
 1209 *Nat. Geosci.*, **12**, 168–173, <https://doi.org/10.1038/s41561-019-0300-3>.

1210 Fekete, B. M., C. J. Vörösmarty, and W. Grabs, 2002: High-resolution fields of global runoff  
 1211 combining observed river discharge and simulated water balances. *Global Biogeochem.*  
 1212 *Cycles*, **16**, 15-1-15–10, <https://doi.org/10.1029/1999gb001254>.

1213 Ferreira, V. G., and Z. Asiah, 2016: An investigation on the closure of the water budget  
 1214 methods over Volta Basin using multi-satellite data. *International Association of*  
 1215 *Geodesy Symposia*, Vol. 144 of, Springer Verlag, 171–178.

1216 Fisher, J. B., and Coauthors, 2017: The future of evapotranspiration: Global requirements for  
 1217 ecosystem functioning, carbon and climate feedbacks, agricultural management, and  
 1218 water resources. *Water Resour. Res.*, **53**, 2618–2626,

- 1219 <https://doi.org/10.1002/2016WR020175>.
- 1220 Flörke, M., E. Kynast, I. Bärlund, S. Eisner, F. Wimmer, and J. Alcamo, 2013: Domestic and  
 1221 industrial water uses of the past 60 years as a mirror of socio-economic development: A  
 1222 global simulation study. *Glob. Environ. Chang.*, **23**, 144–156,  
 1223 <https://doi.org/10.1016/j.gloenvcha.2012.10.018>.
- 1224 Foley, J. A., and Coauthors, 2011: Solutions for a cultivated planet. *Nature*, **478**, 337–342,  
 1225 <https://doi.org/10.1038/nature10452>.
- 1226 Ford, T. W., E. Harris, and S. M. Quiring, 2014: Estimating root zone soil moisture using  
 1227 near-surface observations from SMOS. *Hydrol. Earth Syst. Sci.*, **18**, 139–154,  
 1228 <https://doi.org/10.5194/hess-18-139-2014>.
- 1229 Foster, S., J. Chilton, G. J. Nijsten, and A. Richts, 2013: Groundwater-a global focus on the  
 1230 “local resource.” *Curr. Opin. Environ. Sustain.*, **5**, 685–695,  
 1231 <https://doi.org/10.1016/j.cosust.2013.10.010>.
- 1232 Fowler, H. J., and Coauthors, 2021: Anthropogenic intensification of short-duration rainfall  
 1233 extremes. *Nat. Rev. Earth Environ.*, 1–16, <https://doi.org/10.1038/s43017-020-00128-6>.
- 1234 Frederikse, T., and Coauthors, 2020: The causes of sea-level rise since 1900. *Nature*, **584**,  
 1235 393–397, <https://doi.org/10.1038/s41586-020-2591-3>.
- 1236 Gao, H., C. Birkett, and D. P. Lettenmaier, 2012: Global monitoring of large reservoir storage  
 1237 from satellite remote sensing. *Water Resour. Res.*, **48**,  
 1238 <https://doi.org/10.1029/2012WR012063>.
- 1239 Gardner, A. S., and Coauthors, 2013: A reconciled estimate of glacier contributions to sea  
 1240 level rise: 2003 to 2009. *Science (80-. )*, **340**, 852–857,  
 1241 <https://doi.org/10.1126/science.1234532>.

1242 Gärtner-Roer, I., K. Naegeli, M. Huss, T. Knecht, H. Machguth, and M. Zemp, 2014: A  
 1243 database of worldwide glacier thickness observations. *Glob. Planet. Change*, **122**, 330–  
 1244 344, <https://doi.org/10.1016/j.gloplacha.2014.09.003>.

1245 GCOS, 2015: *Status of the Global Observing System for Climate*. 353 pp.  
 1246 [https://library.wmo.int/index.php?lvl=notice\\_display&id=18962](https://library.wmo.int/index.php?lvl=notice_display&id=18962).

1247 —, 2016: *The Global Observing System for Climate: Implementation needs*. WMO, 235  
 1248 pp.

1249 Gedney, N., P. M. Cox, R. A. Betts, O. Boucher, C. Huntingford, and P. A. Stott, 2006:  
 1250 Detection of a direct carbon dioxide effect in continental river runoff records. *Nature*,  
 1251 **439**, 835–838, <https://doi.org/10.1038/nature04504>.

1252 Gentemann, C. L., and Coauthors, 2020: FluxSat: Measuring the Ocean–Atmosphere  
 1253 Turbulent Exchange of Heat and Moisture from Space. *Remote Sens.*, **12**, 1796,  
 1254 <https://doi.org/10.3390/rs12111796>.

1255 Ghiggi, G., V. Humphrey, S. I. Seneviratne, and L. Gudmundsson, 2019: GRUN: An  
 1256 observation-based global gridded runoff dataset from 1902 to 2014. *Earth Syst. Sci.*  
 1257 *Data*, **11**, 1655–1674, <https://doi.org/10.5194/essd-11-1655-2019>.

1258 Gimeno, L., A. Drumond, R. Nieto, R. M. Trigo, and A. Stohl, 2010: On the origin of  
 1259 continental precipitation. *Geophys. Res. Lett.*, **37**, n/a–n/a,  
 1260 <https://doi.org/10.1029/2010GL043712>.

1261 —, and Coauthors, 2012: Oceanic and terrestrial sources of continental precipitation. *Rev.*  
 1262 *Geophys.*, **50**, <https://doi.org/10.1029/2012RG000389>.

1263 Gleeson, T., K. M. Befus, S. Jasechko, E. Luijendijk, and M. B. Cardenas, 2016: The global  
 1264 volume and distribution of modern groundwater. *Nat. Geosci.*, **9**, 161–164,  
 1265 <https://doi.org/10.1038/ngeo2590>.

- 1266 Gleick, P. H., 1996: Basic water requirements for human activities: Meeting basic needs.  
1267 *Water Int.*, **21**, 83–92, <https://doi.org/10.1080/02508069608686494>.
- 1268 GLIMS and NSIDC, 2005: Global Land Ice Measurements from Space glacier database.  
1269 Compiled and made available by the international GLIMS community and the National  
1270 Snow and Ice Data Center (updated 2018). <https://doi.org/DOI:10.7265/N5V98602>.
- 1271 Gonzalez, R. L., G. Liston, C. Chiu, and B. Notaros, 2019: *THESIS CONSISTENCY IN THE*  
1272 *AMSR-E SNOW PRODUCTS: GROUNDWORK FOR A COUPLED SNOWFALL AND*  
1273 *SWE ALGORITHM*. Colorado State University. Libraries,  
1274 <https://mountainscholar.org/handle/10217/199801> (Accessed September 22, 2020).
- 1275 Goulden, M. L., and R. C. Bales, 2014: Mountain runoff vulnerability to increased  
1276 evapotranspiration with vegetation expansion. *Proc. Natl. Acad. Sci. U. S. A.*, **111**,  
1277 14071–14075, <https://doi.org/10.1073/pnas.1319316111>.
- 1278 de Graaf, I., E. H. Sutanudjaja, L. P. H. van Beek, and M. F. P. Bierkens, 2015: A high-  
1279 resolution global-scale groundwater model. *Hydrol. Earth Syst. Sci.*, **19**, 823–837,  
1280 <https://doi.org/10.5194/hess-19-823-2015>.
- 1281 —, R. van Beek, T. Gleeson, N. Moosdorf, O. Schmitz, E. Sutanudjaja, and M. Bierkens,  
1282 2016: A global-scale two-layer transient groundwater model: development and  
1283 application to groundwater depletion. *Hydrol. Earth Syst. Sci.*, 1–30,  
1284 <https://doi.org/10.5194/hess-2016-121>.
- 1285 Gruber, A., W. A. Dorigo, S. Zwieback, A. Xaver, and W. Wagner, 2013: Characterizing  
1286 Coarse-Scale Representativeness of in situ Soil Moisture Measurements from the  
1287 International Soil Moisture Network. *Vadose Zo. J.*, **12**, vzj2012.0170,  
1288 <https://doi.org/10.2136/vzj2012.0170>.
- 1289 —, T. Scanlon, R. van der Schalie, W. Wagner, and W. Dorigo, 2019: Evolution of the



1290 ESA CCI Soil Moisture climate data records and their underlying merging methodology.  
 1291 *Earth Syst. Sci. Data*, **11**, 717–739, <https://doi.org/10.5194/essd-11-717-2019>.  
 1292 Gutenstein, M., K. Fennig, M. Schröder, T. Trent, S. Bakan, J. B. Roberts, and F. R.  
 1293 Robertson, 2021: Intercomparison of freshwater fluxes over ocean and investigations  
 1294 into water budget closure. *Hydrol. Earth Syst. Sci.*, **25**, 121–146,  
 1295 <https://doi.org/10.5194/hess-25-121-2021>.  
 1296 Haberkorn, A., 2019: *European Snow Booklet*. 363 pp.  
 1297 <https://www.wsl.ch/de/publikationen/european-snow-booklet.html> (Accessed September  
 1298 28, 2020).  
 1299 Harris, I., P. D. Jones, T. J. Osborn, and D. H. Lister, 2014: Updated high-resolution grids of  
 1300 monthly climatic observations - the CRU TS3.10 Dataset. *Int. J. Climatol.*, **34**, 623–642,  
 1301 <https://doi.org/10.1002/joc.3711>.  
 1302 Hegerl, G. C., and Coauthors, 2015: Challenges in quantifying changes in the global water  
 1303 cycle. *Bull. Am. Meteorol. Soc.*, **96**, 1097–1115, [https://doi.org/10.1175/BAMS-D-13-](https://doi.org/10.1175/BAMS-D-13-00212.1)  
 1304 00212.1.  
 1305 Hegglin, M. I., and Coauthors, 2013: SPARC Data Initiative: Comparison of water vapor  
 1306 climatologies from international satellite limb sounders. *J. Geophys. Res. Atmos.*, **118**,  
 1307 11,824–11,846, <https://doi.org/10.1002/jgrd.50752>.  
 1308 Heginbottom, J. A., J. Brown, E. S. Melnikov, and O. J. Ferrians Jr., 1993: Circum-arctic  
 1309 map of permafrost and ground ice conditions. Proceedings of the Sixth International  
 1310 Conference on Permafrost, Wushan, Guangzhou, China Circum-arctic map of permafrost  
 1311 and ground ice conditions. Proceedings of the Sixth International Conference . *South*  
 1312 *China Univ. Press*, **2**, 1132–1136.  
 1313 Held, I. M., and B. J. Soden, 2006: Robust Responses of the Hydrological Cycle to Global

- 1314 Warming. *J. Clim.*, **19**, 5686–5699, <https://doi.org/10.1175/JCLI3990.1>.
- 1315 Herold, M., and Coauthors, 2019: The Role and Need for Space-Based Forest Biomass-  
 1316 Related Measurements in Environmental Management and Policy. *Surv. Geophys.*, **40**,  
 1317 757–778, <https://doi.org/10.1007/s10712-019-09510-6>.
- 1318 Hersbach, H., C. Peubey, A. Simmons, P. Berrisford, P. Poli, and D. Dee, 2015: ERA-20CM:  
 1319 A twentieth-century atmospheric model ensemble. *Q. J. R. Meteorol. Soc.*, **141**, 2350–  
 1320 2375, <https://doi.org/10.1002/qj.2528>.
- 1321 ———, and Coauthors, 2020: The ERA5 global reanalysis. *Q. J. R. Meteorol. Soc.*,  
 1322 <https://doi.org/10.1002/qj.3803>.
- 1323 Heudorfer, B., E. Haaf, K. Stahl, and R. Barthel, 2019: Index- Based Characterization and  
 1324 Quantification of Groundwater Dynamics. *Water Resour. Res.*, **55**, 5575–5592,  
 1325 <https://doi.org/10.1029/2018WR024418>.
- 1326 Hicks, F., and S. Beltaos, 2008: River Ice. *Cold Region Atmospheric and Hydrologic Studies.*  
 1327 *The Mackenzie GEWEX Experience*, Vol. 2 of, Springer Berlin Heidelberg, 281–305.
- 1328 Hirschi, M., and S. I. Seneviratne, 2017: Basin-scale water-balance dataset (BSWB): an  
 1329 update. *Earth Syst. Sci. Data*, **9**, 251–258, <https://doi.org/10.5194/essd-9-251-2017>.
- 1330 Hollmann, R., and Coauthors, 2013: The ESA climate change initiative: Satellite data records  
 1331 for essential climate variables. *Bull. Am. Meteorol. Soc.*, **94**, 1541–1552,  
 1332 <https://doi.org/10.1175/BAMS-D-11-00254.1>.
- 1333 Hosseini, M., and R. Kerachian, 2017: A data fusion-based methodology for optimal redesign  
 1334 of groundwater monitoring networks. *J. Hydrol.*, **552**, 267–282,  
 1335 <https://doi.org/10.1016/j.jhydrol.2017.06.046>.
- 1336 Hou, A. Y., and Coauthors, 2014: The global precipitation measurement mission. *Bull. Am.*

- 1337 *Meteorol. Soc.*, **95**, 701–722, <https://doi.org/10.1175/BAMS-D-13-00164.1>.
- 1338 Huang, C., Y. Chen, S. Zhang, and J. Wu, 2018: Detecting, Extracting, and Monitoring  
1339 Surface Water From Space Using Optical Sensors: A Review. *Rev. Geophys.*, **56**, 333–  
1340 360, <https://doi.org/10.1029/2018RG000598>.
- 1341 Huss, M., 2011: Present and future contribution of glacier storage change to runoff from  
1342 macroscale drainage basins in Europe. *Water Resour. Res.*, **47**,  
1343 <https://doi.org/10.1029/2010WR010299>.
- 1344 —, 2013: Density assumptions for converting geodetic glacier volume change to mass  
1345 change. *Cryosph.*, **7**, 877–887, <https://doi.org/10.5194/tc-7-877-2013>.
- 1346 —, and R. Hock, 2015: A new model for global glacier change and sea-level rise. *Front.*  
1347 *Earth Sci.*, **3**, 54, <https://doi.org/10.3389/feart.2015.00054>.
- 1348 Huuskonen, A., E. Saltikoff, and I. Holleman, 2014: The operational weather radar network  
1349 in Europe. *Bull. Am. Meteorol. Soc.*, **95**, 897–907, [https://doi.org/10.1175/BAMS-D-12-](https://doi.org/10.1175/BAMS-D-12-00216.1)  
1350 00216.1.
- 1351 Idso, S. B., and A. J. Brazel, 1984: Rising atmospheric carbon dioxide concentrations may  
1352 increase streamflow. *Nature*, **312**, 51–53, <https://doi.org/10.1038/312051a0>.
- 1353 IPCC, 2019: *IPCC Special Report on the Ocean and Cryosphere in a Changing Climate*. 1–  
1354 765 pp. <https://www.ipcc.ch/srocc/cite-report/> (Accessed August 26, 2020).
- 1355 Ishii, M., Y. Fukuda, S. Hirahara, S. Yasui, T. Suzuki, and K. Sato, 2017: Accuracy of Global  
1356 Upper Ocean Heat Content Estimation Expected from Present Observational Data Sets.  
1357 *SOLA*, **13**, 163–167, <https://doi.org/10.2151/sola.2017-030>.
- 1358 Jackson, T. J., and T. J. Schmugge, 1991: Vegetation effects on the microwave emission of  
1359 soils. *Remote Sens. Environ.*, **36**, 203–212, <https://doi.org/10.1016/0034->

- 1360 4257(91)90057-D.
- 1361 Jalilvand, E., M. Tajrishy, S. A. Ghazi Zadeh Hashemi, and L. Brocca, 2019: Quantification  
 1362 of irrigation water using remote sensing of soil moisture in a semi-arid region. *Remote*  
 1363 *Sens. Environ.*, **231**, 111226, <https://doi.org/10.1016/j.rse.2019.111226>.
- 1364 Jones, D. B., S. Harrison, K. Anderson, and R. A. Betts, 2018: Mountain rock glaciers  
 1365 contain globally significant water stores. *Sci. Rep.*, **8**, 2834,  
 1366 <https://doi.org/10.1038/s41598-018-21244-w>.
- 1367 Josey, S. A., E. C. Kent, and P. K. Taylor, 1999: New insights into the ocean heat budget  
 1368 closure problem from analysis of the SOC air-sea flux climatology. *J. Clim.*, **12**, 2856–  
 1369 2880, [https://doi.org/10.1175/1520-0442\(1999\)012<2856:NIITOH>2.0.CO;2](https://doi.org/10.1175/1520-0442(1999)012<2856:NIITOH>2.0.CO;2).
- 1370 Jung, M., and Coauthors, 2019: The FLUXCOM ensemble of global land-atmosphere energy  
 1371 fluxes. *Sci. Data*, **6**, 1–14, <https://doi.org/10.1038/s41597-019-0076-8>.
- 1372 Kaser, G., M. Großhauser, and B. Marzeion, 2010: Contribution potential of glaciers to water  
 1373 availability in different climate regimes. *Proc. Natl. Acad. Sci. U. S. A.*, **107**, 20223–  
 1374 20227, <https://doi.org/10.1073/pnas.1008162107>.
- 1375 Kelly, R. E., A. T. Chang, L. Tsang, and J. L. Foster, 2003: A prototype AMSR-E global  
 1376 snow area and snow depth algorithm. *IEEE Trans. Geosci. Remote Sens.*, **41**, 230–242,  
 1377 <https://doi.org/10.1109/TGRS.2003.809118>.
- 1378 Kenway, S., A. Gregory, and J. McMahon, 2011: Urban water mass balance analysis. *J. Ind.*  
 1379 *Ecol.*, **15**, 693–706, <https://doi.org/10.1111/j.1530-9290.2011.00357.x>.
- 1380 Kerr, Y. H., and Coauthors, 2012: The SMOS soil moisture retrieval algorithm. *IEEE Trans.*  
 1381 *Geosci. Remote Sens.*, **50**, 1384–1403, <https://doi.org/10.1109/TGRS.2012.2184548>.
- 1382 Khosrawi, F., and Coauthors, 2018: The SPARC water vapour assessment II: comparison of

1383 stratospheric and lower mesospheric water vapour time series observed from satellites.  
 1384 *Atmos. Meas. Tech.*, **11**, 4435–4463, <https://doi.org/10.5194/amt-11-4435-2018>.

1385 Kidd, C., A. Becker, G. J. Huffman, C. L. Muller, P. Joe, G. Skofronick-Jackson, and D. B.  
 1386 Kirschbaum, 2017: So, how much of the Earth’s surface is covered by rain gauges? *Bull.*  
 1387 *Am. Meteorol. Soc.*, **98**, 69–78, <https://doi.org/10.1175/BAMS-D-14-00283.1>.

1388 Kinzel, P., and C. Legleiter, 2019: sUAS-Based Remote Sensing of River Discharge Using  
 1389 Thermal Particle Image Velocimetry and Bathymetric Lidar. *Remote Sens.*, **11**, 2317,  
 1390 <https://doi.org/10.3390/rs11192317>.

1391 Kittel, C. M. M., 2020: Satellite radar observations for hydrologic and hydrodynamic  
 1392 modelling.

1393 Konikow, L. F., 2011: Contribution of global groundwater depletion since 1900 to sea-level  
 1394 rise. *Geophys. Res. Lett.*, **38**, <https://doi.org/10.1029/2011GL048604>.

1395 Konings, A. G., and M. Momen, 2018: Frequency-dependence of vegetation optical depth-  
 1396 derived isohydricity estimates. *International Geoscience and Remote Sensing Symposium*  
 1397 *(IGARSS)*, Vol. 2018-July of, Institute of Electrical and Electronics Engineers Inc.,  
 1398 9045–9047.

1399 Kooperman, G. J., M. D. Fowler, F. M. Hoffman, C. D. Koven, K. Lindsay, M. S. Pritchard,  
 1400 A. L. S. Swann, and J. T. Randerson, 2018: Plant Physiological Responses to Rising CO  
 1401 <sub>2</sub> Modify Simulated Daily Runoff Intensity With Implications for Global- Scale Flood  
 1402 Risk Assessment. *Geophys. Res. Lett.*, **45**, 12,457-12,466,  
 1403 <https://doi.org/10.1029/2018GL079901>.

1404 Korzoun, V. I. (ed. . V., and Coauthors, 1978: *World water balance and water resources of*  
 1405 *the Earth*. UNESCO Press,.

1406 Koutsoyiannis, D., 2020: Revisiting the global hydrological cycle: is it intensifying? *Hydrol.*

1407 *Earth Syst. Sci.*, **24**, 3899–3932, <https://doi.org/10.5194/hess-24-3899-2020>.

1408 Kumar, S. V., C. D. Peters-Lidard, J. A. Santanello, R. H. Reichle, C. S. Draper, R. D.

1409 Koster, G. Nearing, and M. F. Jasinski, 2015: Evaluating the utility of satellite soil

1410 moisture retrievals over irrigated areas and the ability of land data assimilation methods

1411 to correct for unmodeled processes. *Hydrol. Earth Syst. Sci.*, **19**, 4463–4478,

1412 <https://doi.org/10.5194/hess-19-4463-2015>.

1413 Landerer, F. W., J. O. Dickey, and A. Güntner, 2010: Terrestrial water budget of the Eurasian

1414 pan-Arctic from GRACE satellite measurements during 2003-2009. *J. Geophys. Res.*

1415 *Atmos.*, **115**, <https://doi.org/10.1029/2010JD014584>.

1416 Landwehr, S., N. O’Sullivan, and B. Ward, 2015: Direct flux measurements from mobile

1417 platforms at sea: Motion and airflow distortion corrections revisited. *J. Atmos. Ocean.*

1418 *Technol.*, **32**, 1163–1178, <https://doi.org/10.1175/JTECH-D-14-00137.1>.

1419 Lawford, R. G., and Coauthors, 2004: Advancing global-and continental-scale

1420 hydrometeorology: Contributions of GEWEX hydrometeorology panel. *Bull. Am.*

1421 *Meteorol. Soc.*, **85**, 1917–1930, <https://doi.org/10.1175/BAMS-85-12-1917>.

1422 Lemordant, L., and P. Gentile, 2019: Vegetation Response to Rising CO<sub>2</sub> Impacts Extreme

1423 Temperatures. *Geophys. Res. Lett.*, **46**, 1383–1392,

1424 <https://doi.org/10.1029/2018GL080238>.

1425 Levitus, S., and Coauthors, 2012: World ocean heat content and thermosteric sea level

1426 change (0-2000m), 1955-2010. *Geophys. Res. Lett.*, **39**,

1427 <https://doi.org/10.1029/2012GL051106>.

1428 Li, B., and Coauthors, 2019: Global GRACE Data Assimilation for Groundwater and

1429 Drought Monitoring: Advances and Challenges. *Water Resour. Res.*, **55**, 7564–7586,

1430 <https://doi.org/10.1029/2018WR024618>.

- 1431 Lievens, H., and Coauthors, 2019: Snow depth variability in the Northern Hemisphere  
 1432 mountains observed from space. *Nat. Commun.*, **10**, 1–12,  
 1433 <https://doi.org/10.1038/s41467-019-12566-y>.
- 1434 Liman, J., M. Schröder, K. Fennig, A. Andersson, and R. Hollmann, 2018: Uncertainty  
 1435 characterization of HOAPS 3.3 latent heat-flux-related parameters. *Atmos. Meas. Tech.*,  
 1436 **11**, 1793–1815, <https://doi.org/10.5194/amt-11-1793-2018>.
- 1437 Liu, W., and Coauthors, 2018: Investigating water budget dynamics in 18 river basins across  
 1438 the Tibetan Plateau through multiple datasets. *Hydrol. Earth Syst. Sci.*, **22**, 351–371,  
 1439 <https://doi.org/10.5194/hess-22-351-2018>.
- 1440 Liu, W. T., K. B. Katsaros, and J. A. Businger, 1979: Bulk parameterization of air-sea  
 1441 exchanges of heat and water vapor including the molecular constraints at the interface. *J.*  
 1442 *Atmos. Sci.*, **36**, 1722–1735, [https://doi.org/10.1175/1520-](https://doi.org/10.1175/1520-0469(1979)036<1722:BPOASE>2.0.CO;2)  
 1443 [0469\(1979\)036<1722:BPOASE>2.0.CO;2](https://doi.org/10.1175/1520-0469(1979)036<1722:BPOASE>2.0.CO;2).
- 1444 Llovel, W., S. Purkey, B. Meyssignac, A. Blazquez, N. Kolodziejczyk, and J. Bamber, 2019:  
 1445 Global ocean freshening, ocean mass increase and global mean sea level rise over 2005–  
 1446 2015. *Sci. Rep.*, **9**, <https://doi.org/10.1038/s41598-019-54239-2>.
- 1447 Lopez, O., and Coauthors, 2020: Mapping groundwater abstractions from irrigated  
 1448 agriculture: big data, inverse modeling and a satellite-model fusion approach. *Hydrol.*  
 1449 *Earth Syst. Sci. Discuss.*, 1–41, <https://doi.org/10.5194/hess-2020-50>.
- 1450 Luck, M., M. Landis, and F. Gassert, 2015: *Aqueduct Water Stress Projections: Decadal*  
 1451 *Projections Of Water Supply And Demand Using CMIP5 GCMs*.  
 1452 <https://pdfs.semanticscholar.org/e41a/facfea14a74ebf839c3e71d01ff7466fe683.pdf>  
 1453 (Accessed September 28, 2020).
- 1454 Luijendijk, E., T. Gleeson, and N. Moosdorf, 2020: Fresh groundwater discharge

1455 insignificant for the world's oceans but important for coastal ecosystems. *Nat.*  
 1456 *Commun.*, **11**, 1–12, <https://doi.org/10.1038/s41467-020-15064-8>.

1457 Luo, Z., Q. Shao, W. Wan, H. Li, X. Chen, S. Zhu, and X. Ding, 2021: A new method for  
 1458 assessing satellite-based hydrological data products using water budget closure. *J.*  
 1459 *Hydrol.*, **594**, 125927, <https://doi.org/10.1016/j.jhydrol.2020.125927>.

1460 Makiyara, Y., 1996: A Method for Improving Radar Estimates of Precipitation by Comparing  
 1461 Data from Radars and Raingauges. *J. Meteorol. Soc. Japan. Ser. II*, **74**, 459–480,  
 1462 [https://doi.org/10.2151/jmsj1965.74.4\\_459](https://doi.org/10.2151/jmsj1965.74.4_459).

1463 Mariotti, A., M. V. Struglia, N. Zeng, and K. M. Lau, 2002: The hydrological cycle in the  
 1464 Mediterranean region and implications for the water budget of the Mediterranean sea. *J.*  
 1465 *Clim.*, **15**, 1674–1690, [https://doi.org/10.1175/1520-](https://doi.org/10.1175/1520-0442(2002)015<1674:THCITM>2.0.CO;2)  
 1466 [0442\(2002\)015<1674:THCITM>2.0.CO;2](https://doi.org/10.1175/1520-0442(2002)015<1674:THCITM>2.0.CO;2).

1467 Martens, B., and Coauthors, 2017: GLEAM v3: satellite-based land evaporation and root-  
 1468 zone soil moisture. *Geosci. Model Dev.*, **10**, 1903–1925, [https://doi.org/10.5194/gmd-](https://doi.org/10.5194/gmd-10-1903-2017)  
 1469 [10-1903-2017](https://doi.org/10.5194/gmd-10-1903-2017).

1470 ———, R. de Jeu, N. Verhoest, H. Schuurmans, J. Kleijer, and D. Miralles, 2018: Towards  
 1471 Estimating Land Evaporation at Field Scales Using GLEAM. *Remote Sens.*, **10**, 1720,  
 1472 <https://doi.org/10.3390/rs10111720>.

1473 Marvel, K., B. I. Cook, C. J. W. Bonfils, P. J. Durack, J. E. Smerdon, and A. P. Williams,  
 1474 2019: Twentieth-century hydroclimate changes consistent with human influence.  
 1475 *Nature*, **569**, 59–65, <https://doi.org/10.1038/s41586-019-1149-8>.

1476 Massari, C., and Coauthors, 2020: A daily 25 km short-latency rainfall product for data-  
 1477 scarce regions based on the integration of the Global Precipitation Measurement mission  
 1478 rainfall and multiple-satellite soil moisture products. *Hydrol. Earth Syst. Sci.*, **24**, 2687–



1479 2710, <https://doi.org/10.5194/hess-24-2687-2020>.

1480 Masunaga, H., M. Schröder, F. A. Furuzawa, C. Kummerow, E. Rustemeier, and U.  
 1481 Schneider, 2019: Inter-product biases in global precipitation extremes. *Environ. Res.*  
 1482 *Lett.*, **14**, 125016, <https://doi.org/10.1088/1748-9326/ab5da9>.

1483 McCabe, M. F., A. Ershadi, C. Jimenez, D. G. Miralles, D. Michel, and E. F. Wood, 2016:  
 1484 The GEWEX LandFlux project: evaluation of model evaporation using tower-based and  
 1485 globally gridded forcing data. *Geosci. Model Dev.*, **9**, 283–305,  
 1486 <https://doi.org/10.5194/gmd-9-283-2016>.

1487 ———, D. G. Miralles, T. R. H. Holmes, and J. B. Fisher, 2019: Advances in the Remote  
 1488 Sensing of Terrestrial Evaporation. *Remote Sens.*, **11**, 1138,  
 1489 <https://doi.org/10.3390/rs11091138>.

1490 Milliman, J. D., and K. L. Farnsworth, 2011: *River discharge to the coastal ocean: A global*  
 1491 *synthesis*. Cambridge University Press, 1–384 pp.

1492 Miralles, D. G., R. A. M. De Jeu, J. H. Gash, T. R. H. Holmes, and A. J. Dolman, 2011:  
 1493 Magnitude and variability of land evaporation and its components at the global scale.  
 1494 *Hydrol. Earth Syst. Sci.*, **15**, 967–981, <https://doi.org/10.5194/hess-15-967-2011>.

1495 ———, and Coauthors, 2016: The WACMOS-ET project &ndash; Part 2: Evaluation of  
 1496 global terrestrial evaporation data sets. *Hydrol. Earth Syst. Sci.*, **20**, 823–842,  
 1497 <https://doi.org/10.5194/hess-20-823-2016>.

1498 ———, P. Gentile, S. I. Seneviratne, and A. J. Teuling, 2019: Land–atmospheric feedbacks  
 1499 during droughts and heatwaves: state of the science and current challenges. *Ann. N. Y.*  
 1500 *Acad. Sci.*, **1436**, 19–35, <https://doi.org/10.1111/nyas.13912>.

1501 Mitchell, A. L., A. Rosenqvist, and B. Mora, 2017: Current remote sensing approaches to  
 1502 monitoring forest degradation in support of countries measurement, reporting and

1503 verification (MRV) systems for REDD+. *Carbon Balance Manag.*, **12**, 9,  
 1504 <https://doi.org/10.1186/s13021-017-0078-9>.

1505 Moesinger, L., W. Dorigo, R. de Jeu, R. van der Schalie, T. Scanlon, I. Teubner, and M.  
 1506 Forkel, 2020: The global long-term microwave Vegetation Optical Depth Climate  
 1507 Archive (VODCA). *Earth Syst. Sci. Data*, **12**, 177–196, [https://doi.org/10.5194/essd-12-](https://doi.org/10.5194/essd-12-177-2020)  
 1508 177-2020.

1509 Mohan, C., A. W. Western, Y. Wei, and M. Saft, 2018: Predicting groundwater recharge for  
 1510 varying land cover and climate conditions – a global meta-study. *Hydrol. Earth Syst.*  
 1511 *Sci.*, **22**, 2689–2703, <https://doi.org/10.5194/hess-22-2689-2018>.

1512 Moholdt, G., B. Wouters, and A. S. Gardner, 2012: Recent mass changes of glaciers in the  
 1513 Russian High Arctic. *Geophys. Res. Lett.*, **39**, n/a-n/a,  
 1514 <https://doi.org/10.1029/2012GL051466>.

1515 Mokany, K., R. J. Raison, and A. S. Prokushkin, 2006: Critical analysis of root: Shoot ratios  
 1516 in terrestrial biomes. *Glob. Chang. Biol.*, **12**, 84–96, [https://doi.org/10.1111/j.1365-](https://doi.org/10.1111/j.1365-2486.2005.001043.x)  
 1517 2486.2005.001043.x.

1518 Moninger, W. R., S. G. Benjamin, B. D. Jamison, T. W. Schlatter, T. L. Smith, and E. J.  
 1519 Szoke, 2010: Evaluation of regional aircraft observations using TAMDAR. *Weather*  
 1520 *Forecast.*, **25**, 627–645, <https://doi.org/10.1175/2009WAF2222321.1>.

1521 Moreira, A. A., A. L. Ruhoff, D. R. Roberti, V. de A. Souza, H. R. da Rocha, and R. C. D. de  
 1522 Paiva, 2019: Assessment of terrestrial water balance using remote sensing data in South  
 1523 America. *J. Hydrol.*, **575**, 131–147, <https://doi.org/10.1016/j.jhydrol.2019.05.021>.

1524 Morrow, R., and Coauthors, 2019: Global observations of fine-scale ocean surface  
 1525 topography with the Surface Water and Ocean Topography (SWOT) Mission. *Front.*  
 1526 *Mar. Sci.*, **6**, <https://doi.org/10.3389/fmars.2019.00232>.

- 1527 Mortimer, C., L. Mudryk, C. Derksen, K. Luojus, R. Brown, R. Kelly, and M. Tedesco, 2020:  
1528 Evaluation of long-term Northern Hemisphere snow water equivalent products.  
1529 *Cryosph.*, **14**, 1579–1594, <https://doi.org/10.5194/tc-14-1579-2020>.
- 1530 Munier, S., F. Aires, S. Schlaffer, C. Prigent, F. Papa, P. Maisongrande, and M. Pan, 2014:  
1531 Combining data sets of satellite-retrieved products for basin-scale water balance study:  
1532 2. Evaluation on the Mississippi Basin and closure correction model. *J. Geophys. Res.*  
1533 *Atmos.*, **119**, 12,100–12,116, <https://doi.org/10.1002/2014JD021953>.
- 1534 ———, ———, and F. Aires, 2018: A new global method of satellite dataset merging and quality  
1535 characterization constrained by the terrestrial water budget. *Remote Sens. Environ.*, **205**,  
1536 119–130, <https://doi.org/10.1016/j.rse.2017.11.008>.
- 1537 National Academies of Sciences, 2016: *Attribution of Extreme Weather Events in the Context*  
1538 *of Climate Change*. The National Academies Press,.
- 1539 Ning, S., H. Ishidaira, and J. Wang, 2014: Statistical downscaling of grace-derived terrestrial  
1540 water storage using satellite and gldas products. *J. Japan Soc. Civ. Eng. Ser. B1*  
1541 *(Hydraulic Eng.)*, **70**, I\_133–I\_138, [https://doi.org/10.2208/jscejhe.70.i\\_133](https://doi.org/10.2208/jscejhe.70.i_133).
- 1542 Oki, T., 1999: The global water cycle. *In Global Energy and Water Cycles*, Browning K. and  
1543 G. R., Eds., 10–27.
- 1544 ———, and S. Kanae, 2006: Global hydrological cycles and world water resources. *Science*  
1545 *(80-. )*, **313**, 1068–1072, <https://doi.org/10.1126/science.1128845>.
- 1546 Padrón, R. S., and Coauthors, 2020: Observed changes in dry-season water availability  
1547 attributed to human-induced climate change. *Nat. Geosci.*, **13**, 477–481,  
1548 <https://doi.org/10.1038/s41561-020-0594-1>.
- 1549 Pan, M., and E. F. Wood, 2006: Data assimilation for estimating the terrestrial water budget  
1550 using a constrained ensemble Kalman filter. *J. Hydrometeorol.*, **7**, 534–547,

1551 <https://doi.org/10.1175/JHM495.1>.

1552 ———, A. K. Sahoo, T. J. Troy, R. K. Vinukollu, J. Sheffield, and A. E. F. Wood, 2012:

1553 Multisource estimation of long-term terrestrial water budget for major global river

1554 basins. *J. Clim.*, **25**, 3191–3206, <https://doi.org/10.1175/JCLI-D-11-00300.1>.

1555 Pan, S., and Coauthors, 2020: Evaluation of global terrestrial evapotranspiration using state-

1556 of-the-art approaches in remote sensing, machine learning and land surface modeling.

1557 *Hydrol. Earth Syst. Sci.*, **24**, 1485–1509, <https://doi.org/10.5194/hess-24-1485-2020>.

1558 Paul, F., and Coauthors, 2009: Recommendations for the compilation of glacier inventory

1559 data from digital sources. *Ann. Glaciol.*, **50**, 119–126,

1560 <https://doi.org/10.3189/172756410790595778>.

1561 Pellarin, T., and Coauthors, 2020: The Precipitation Inferred from Soil Moisture (PrISM)

1562 Near Real-Time Rainfall Product: Evaluation and Comparison. *Remote Sens.*, **12**, 481,

1563 <https://doi.org/10.3390/rs12030481>.

1564 Pellet, V., F. Aires, S. Munier, D. Fernández Prieto, G. Jordá, W. A. Dorigo, J. Polcher, and

1565 L. Brocca, 2019: Integrating multiple satellite observations into a coherent dataset to

1566 monitor the full water cycle – application to the Mediterranean region. *Hydrol. Earth*

1567 *Syst. Sci.*, **23**, 465–491, <https://doi.org/10.5194/hess-23-465-2019>.

1568 ———, ———, F. Papa, S. Munier, and B. Decharme, 2020: Long-term total water storage

1569 change from a Satellite Water Cycle reconstruction over large southern Asian basins.

1570 *Hydrol. Earth Syst. Sci.*, **24**, 3033–3055, <https://doi.org/10.5194/hess-24-3033-2020>.

1571 Peña-Arancibia, J. L., L. A. Bruijnzeel, M. Mulligan, and A. I. J. M. van Dijk, 2019: Forests

1572 as ‘sponges’ and ‘pumps’: Assessing the impact of deforestation on dry-season flows

1573 across the tropics. *J. Hydrol.*, **574**, 946–963,

1574 <https://doi.org/10.1016/j.jhydrol.2019.04.064>.

- 1575 Penman, J., and Coauthors, 2003: *Good Practice Guidance for Land Use, Land-Use Change*  
 1576 *and Forestry*. 590 pp.
- 1577 Petersen, W., and Coauthors, 2016: *GPM Level 1 Science Requirements: Science and*  
 1578 *Performance Viewed from the Ground*. NASA Technical Reports Server.  
 1579 <https://ntrs.nasa.gov/citations/20160012025> (Accessed August 26, 2020).
- 1580 Petzold, A., and Coauthors, 2015: Global-scale atmosphere monitoring by in-service aircraft -  
 1581 current achievements and future prospects of the European Research Infrastructure  
 1582 IAGOS. *Tellus, Ser. B Chem. Phys. Meteorol.*, **6**, 1–24,  
 1583 <https://doi.org/10.3402/tellusb.v67.28452>.
- 1584 Pfahl, S., P. A. O’Gorman, and E. M. Fischer, 2017: Understanding the regional pattern of  
 1585 projected future changes in extreme precipitation. *Nat. Clim. Chang.*, **7**, 423–427,  
 1586 <https://doi.org/10.1038/nclimate3287>.
- 1587 Popp, T., and Coauthors, 2020: Consistency of satellite climate data records for Earth system  
 1588 monitoring. *Bull. Am. Meteorol. Soc.*, **preprint**, [https://doi.org/10.1175/bams-d-19-](https://doi.org/10.1175/bams-d-19-0127.1)  
 1589 [0127.1](https://doi.org/10.1175/bams-d-19-0127.1).
- 1590 Preimesberger, W., T. Scanlon, C.-H. Su, A. Gruber, and W. Dorigo, 2020: Homogenization  
 1591 of Structural Breaks in the Global ESA CCI Soil Moisture Multisatellite Climate Data  
 1592 Record. *IEEE Trans. Geosci. Remote Sens.*, 1–18,  
 1593 <https://doi.org/10.1109/tgrs.2020.3012896>.
- 1594 Pritchard, H. D., 2019: Asia’s shrinking glaciers protect large populations from drought  
 1595 stress. *Nature*, **569**, 649–654, <https://doi.org/10.1038/s41586-019-1240-1>.
- 1596 Prytherch, J., E. C. Kent, S. Fangohr, and D. I. Berry, 2015: A comparison of SSM/I-derived  
 1597 global marine surface-specific humidity datasets. *Int. J. Climatol.*, **35**, 2359–2381,  
 1598 <https://doi.org/10.1002/joc.4150>.

1599 Pulliainen, J., 2006: Mapping of snow water equivalent and snow depth in boreal and sub-  
 1600 arctic zones by assimilating space-borne microwave radiometer data and ground-based  
 1601 observations. *Remote Sens. Environ.*, **101**, 257–269,  
 1602 <https://doi.org/10.1016/j.rse.2006.01.002>.  
 1603 —, and Coauthors, 2020: Patterns and trends of Northern Hemisphere snow mass from  
 1604 1980 to 2018. *Nature*, **581**, 294–298, <https://doi.org/10.1038/s41586-020-2258-0>.  
 1605 Raj, R. P., and Coauthors, 2020: Arctic Sea Level Budget Assessment during the  
 1606 GRACE/Argo Time Period. *Remote Sens.*, **12**, 2837,  
 1607 <https://doi.org/10.3390/rs12172837>.  
 1608 Rast, M., J. Johannessen, and W. Mauser, 2014: Review of Understanding of Earth's  
 1609 Hydrological Cycle: Observations, Theory and Modelling. 491–513.  
 1610 Reinecke, R., L. Foglia, S. Mehl, T. Trautmann, D. Cáceres, and P. Döll, 2019: Challenges in  
 1611 developing a global gradient-based groundwater model  
 1612 (G&lt;sup&gt;3&lt;/sup>M v1.0) for the integration into a global  
 1613 hydrological model. *Geosci. Model Dev.*, **12**, 2401–2418, [https://doi.org/10.5194/gmd-](https://doi.org/10.5194/gmd-12-2401-2019)  
 1614 12-2401-2019.  
 1615 Reul, N., and Coauthors, 2020: Sea surface salinity estimates from spaceborne L-band  
 1616 radiometers: An overview of the first decade of observation (2010–2019). *Remote Sens.*  
 1617 *Environ.*, **242**, 111769, <https://doi.org/10.1016/j.rse.2020.111769>.  
 1618 RGI, 2017: Randolph Glacier Inventory 6.0, technical report. [https://doi.org/10.7265/n5-rgi-](https://doi.org/10.7265/n5-rgi-60)  
 1619 60.  
 1620 Robertson, F. R., and Coauthors, 2020: Uncertainties in ocean latent heat flux variations over  
 1621 recent decades in satellite-based estimates and reduced observation reanalyses. *J. Clim.*,  
 1622 **33**, 8415–8437, <https://doi.org/10.1175/JCLI-D-19-0954.1>.

1623 Robock, A., K. Y. Vinnikov, G. Srinivasan, J. K. Entin, S. E. Hollinger, N. A. Speranskaya,  
 1624 S. Liu, and A. Namkhai, 2000: The Global Soil Moisture Data Bank. *Bull. Am.*  
 1625 *Meteorol. Soc.*, **81**, 1281–1299, <https://doi.org/10.1175/1520->  
 1626 [0477\(2000\)081<1281:TGSMDB>2.3.CO;2](https://doi.org/10.1175/1520-0477(2000)081<1281:TGSMDB>2.3.CO;2).  
 1627 Rodell, M., J. S. Famiglietti, J. Chen, S. I. Seneviratne, P. Viterbo, S. Holl, and C. R. Wilson,  
 1628 2004: Basin scale estimates of evapotranspiration using GRACE and other observations.  
 1629 *Geophys. Res. Lett.*, **31**, <https://doi.org/10.1029/2004GL020873>.  
 1630 ———, E. B. McWilliams, J. S. Famiglietti, H. K. Beaudoin, and J. Nigro, 2011: Estimating  
 1631 evapotranspiration using an observation based terrestrial water budget. *Hydrol. Process.*,  
 1632 **25**, 4082–4092, <https://doi.org/10.1002/hyp.8369>.  
 1633 ———, and Coauthors, 2015: The observed state of the water cycle in the early twenty-first  
 1634 century. *J. Clim.*, **28**, 8289–8318, <https://doi.org/10.1175/JCLI-D-14-00555.1>.  
 1635 ———, J. S. Famiglietti, D. N. Wiese, J. T. Reager, H. K. Beaudoin, F. W. Landerer, and M.  
 1636 H. Lo, 2018: Emerging trends in global freshwater availability. *Nature*, **557**, 651–659,  
 1637 <https://doi.org/10.1038/s41586-018-0123-1>.  
 1638 Sadat-Noori, M., I. R. Santos, C. J. Sanders, L. M. Sanders, and D. T. Maher, 2015:  
 1639 Groundwater discharge into an estuary using spatially distributed radon time series and  
 1640 radium isotopes. *J. Hydrol.*, **528**, 703–719,  
 1641 <https://doi.org/10.1016/j.jhydrol.2015.06.056>.  
 1642 Sahely, H. R., S. Dudding, and C. A. Kennedy, 2003: Estimating the urban metabolism of  
 1643 Canadian cities: Greater Toronto Area case study. *Can. J. Civ. Eng.*, **30**, 468–483,  
 1644 <https://doi.org/10.1139/102-105>.  
 1645 Sahoo, A. K., M. Pan, T. J. Troy, R. K. Vinukollu, J. Sheffield, and E. F. Wood, 2011:  
 1646 Reconciling the global terrestrial water budget using satellite remote sensing. *Remote*

1647 *Sens. Environ.*, **115**, 1850–1865, <https://doi.org/10.1016/j.rse.2011.03.009>.

1648 Saltikoff, E., and Coauthors, 2019: An overview of using weather radar for climatological  
 1649 studies successes, challenges, and potential. *Bull. Am. Meteorol. Soc.*, **100**, 1739–1751,  
 1650 <https://doi.org/10.1175/BAMS-D-18-0166.1>.

1651 Schmied, H. M., and Coauthors, 2020: The global water resources and use model WaterGAP  
 1652 v2.2d: Model description and evaluation. *Geosci. Model Dev.*,  
 1653 <https://doi.org/10.5194/gmd-2020-225>.

1654 Schmitt, R. W., 1995: The ocean component of the global water cycle. *Rev. Geophys.*, **33**,  
 1655 1395–1409, <https://doi.org/10.1029/95RG00184>.

1656 Schneider, U., A. Becker, P. Finger, A. Meyer-Christoffer, M. Ziese, and B. Rudolf, 2014:  
 1657 GPCC's new land surface precipitation climatology based on quality-controlled in situ  
 1658 data and its role in quantifying the global water cycle. *Theor. Appl. Climatol.*, **115**, 15–  
 1659 40, <https://doi.org/10.1007/s00704-013-0860-x>.

1660 —, P. Finger, A. Meyer-Christoffer, E. Rustemeier, M. Ziese, and A. Becker, 2017:  
 1661 Evaluating the Hydrological Cycle over Land Using the Newly-Corrected Precipitation  
 1662 Climatology from the Global Precipitation Climatology Centre (GPCC). *Atmosphere*  
 1663 *(Basel)*, **8**, 52, <https://doi.org/10.3390/atmos8030052>.

1664 Schröder, M., M. Lockhoff, J. M. Forsythe, H. Q. Cronk, T. H. V. Haar, and R. Bennartz,  
 1665 2016: The GEWEX water vapor assessment: Results from intercomparison, trend, and  
 1666 homogeneity analysis of total column water vapor. *J. Appl. Meteorol. Climatol.*, **55**,  
 1667 1633–1649, <https://doi.org/10.1175/jamc-d-15-0304.1>.

1668 —, and Coauthors, 2018: The GEWEX Water Vapor Assessment archive of water vapour  
 1669 products from satellite observations and reanalyses. *Earth Syst. Sci. Data*, **10**, 1093–  
 1670 1117, <https://doi.org/10.5194/essd-10-1093-2018>.



1671 Seneviratne, S. I., T. Corti, E. L. Davin, M. Hirschi, E. B. Jaeger, I. Lehner, B. Orlowsky, and  
 1672 A. J. Teuling, 2010: Investigating soil moisture-climate interactions in a changing  
 1673 climate: A review. *Earth-Science Rev.*, **99**, 125–161,  
 1674 <https://doi.org/10.1016/j.earscirev.2010.02.004>.  
 1675 Sheffield, J., C. R. Ferguson, T. J. Troy, E. F. Wood, and M. F. McCabe, 2009: Closing the  
 1676 terrestrial water budget from satellite remote sensing. *Geophys. Res. Lett.*, **36**,  
 1677 <https://doi.org/10.1029/2009GL037338>.  
 1678 Shepherd, A., and Coauthors, 2018: Mass balance of the Antarctic Ice Sheet from 1992 to  
 1679 2017. *Nature*, **558**, 219–222, <https://doi.org/10.1038/s41586-018-0179-y>.  
 1680 ———, and Coauthors, 2020: Mass balance of the Greenland Ice Sheet from 1992 to 2018.  
 1681 *Nature*, **579**, 233–239, <https://doi.org/10.1038/s41586-019-1855-2>.  
 1682 Shige, S., and C. D. Kummerow, 2016: Precipitation-top heights of heavy orographic rainfall  
 1683 in the Asian monsoon region. *J. Atmos. Sci.*, **73**, 3009–3024,  
 1684 <https://doi.org/10.1175/JAS-D-15-0271.1>.  
 1685 Shiklomanov, I., and J. Rodda, 2004: World water resources at the beginning of the twenty-  
 1686 first century. *Choice Rev. Online*, **41**, 41-4063-41-4063,  
 1687 <https://doi.org/10.5860/choice.41-4063>.  
 1688 Shiklomanov, I. A., 2000: Appraisal and Assessment of world water resources. *Water Int.*,  
 1689 **25**, 11–32, <https://doi.org/10.1080/02508060008686794>.  
 1690 ———, 2008: *Water resources of Russia and their use*. 600 pp.  
 1691 ———, S. Déry, M. Tretiakov, D. Yang, D. Magritsky, A. Georgiadi, and W. Tang, 2021:  
 1692 River Freshwater Flux to the Arctic Ocean. *Arctic Hydrology, Permafrost and*  
 1693 *Ecosystems*, Springer International Publishing, 703–738.

- 1694 Siebert, S., and P. Döll, 2010: Quantifying blue and green virtual water contents in global  
1695 crop production as well as potential production losses without irrigation. *J. Hydrol.*, **384**,  
1696 198–217, <https://doi.org/10.1016/j.jhydrol.2009.07.031>.
- 1697 Singh, P., and L. Bengtsson, 2004: Hydrological sensitivity of a large Himalayan basin to  
1698 climate change. *Hydrol. Process.*, **18**, 2363–2385, <https://doi.org/10.1002/hyp.1468>.
- 1699 Slater, T., A. E. Hogg, and R. Mottram, 2020: Ice-sheet losses track high-end sea-level rise  
1700 projections. *Nat. Clim. Chang.*, 1–3, <https://doi.org/10.1038/s41558-020-0893-y>.
- 1701 Spawn, S. A., C. C. Sullivan, T. J. Lark, and H. K. Gibbs, 2020: Harmonized global maps of  
1702 above and belowground biomass carbon density in the year 2010. *Sci. Data*, **7**, 1–22,  
1703 <https://doi.org/10.1038/s41597-020-0444-4>.
- 1704 Srinivasamoorthy, K., G. Ponnumani, R. Prakash, S. Gopinath, K. Saravanan, and F.  
1705 Vinnarasi, 2019: Tracing groundwater inputs to Bay of Bengal from Sankarabarani  
1706 River Basin, Pondicherry, India, using continuous radon monitoring. *Int. J. Environ. Sci.*  
1707 *Technol.*, **16**, 5513–5524, <https://doi.org/10.1007/s13762-018-1938-x>.
- 1708 Stefan, C., and N. Ansems, 2018: Web-based global inventory of managed aquifer recharge  
1709 applications. *Sustain. Water Resour. Manag.*, **4**, 153–162,  
1710 <https://doi.org/10.1007/s40899-017-0212-6>.
- 1711 Stephens, G. L., and Coauthors, 2012: An update on Earth’s energy balance in light of the  
1712 latest global observations. *Nat. Geosci.*, **5**, 691–696, <https://doi.org/10.1038/ngeo1580>.
- 1713 Stickler, A., and Coauthors, 2010: The comprehensive historical upper-air network. *Bull. Am.*  
1714 *Meteorol. Soc.*, **91**, 741–751, <https://doi.org/10.1175/2009BAMS2852.1>.
- 1715 Swenson, S., and J. Wahr, 2009: Monitoring the water balance of Lake Victoria, East Africa,  
1716 from space. *J. Hydrol.*, **370**, 163–176, <https://doi.org/10.1016/j.jhydrol.2009.03.008>.

- 1717 Syed, T. H., J. S. Famiglietti, V. Zlotnicki, and M. Rodell, 2007: Contemporary estimates of  
1718 Pan-Arctic freshwater discharge from GRACE and reanalysis. *Geophys. Res. Lett.*, **34**,  
1719 L19404, <https://doi.org/10.1029/2007GL031254>.
- 1720 Szeto, K. K., 2007: Assessing Water and Energy Budgets for the Saskatchewan River Basin.  
1721 *J. Meteorol. Soc. Japan*, **85A**, 167–186, <https://doi.org/10.2151/jmsj.85A.167>.
- 1722 ———, R. E. Stewart, M. K. Yau, and J. Gyakum, 2008: The Mackenzie climate system: A  
1723 synthesis of MAGS atmospheric research. *Cold Region Atmospheric and Hydrologic*  
1724 *Studies. The Mackenzie GEWEX Experience: Volume 1: Atmospheric Dynamics*,  
1725 Springer Berlin Heidelberg, 23–50.
- 1726 Takala, M., K. Luojus, J. Pulliainen, C. Derksen, J. Lemmetyinen, J. P. Kärnä, J. Koskinen,  
1727 and B. Bojkov, 2011: Estimating northern hemisphere snow water equivalent for climate  
1728 research through assimilation of space-borne radiometer data and ground-based  
1729 measurements. *Remote Sens. Environ.*, **115**, 3517–3529,  
1730 <https://doi.org/10.1016/j.rse.2011.08.014>.
- 1731 ———, J. Ikonen, K. Luojus, J. Lemmetyinen, S. Metsamäki, J. Cohen, A. N. Arslan, and J.  
1732 Pulliainen, 2017: New Snow Water Equivalent Processing System with Improved  
1733 Resolution over Europe and its Applications in Hydrology. *IEEE J. Sel. Top. Appl.*  
1734 *Earth Obs. Remote Sens.*, **10**, 428–436, <https://doi.org/10.1109/JSTARS.2016.2586179>.
- 1735 Talsma, C. J., S. P. Good, C. Jimenez, B. Martens, J. B. Fisher, D. G. Miralles, M. F.  
1736 McCabe, and A. J. Purdy, 2018: Partitioning of evapotranspiration in remote sensing-  
1737 based models. *Agric. For. Meteorol.*, **260–261**, 131–143,  
1738 <https://doi.org/10.1016/j.agrformet.2018.05.010>.
- 1739 Tarek, M., F. P. Brissette, and R. Arsenault, 2020: Evaluation of the ERA5 reanalysis as a  
1740 potential reference dataset for hydrological modelling over North America. *Hydrol.*

- 1741 *Earth Syst. Sci.*, **24**, 2527–2544, <https://doi.org/10.5194/hess-24-2527-2020>.
- 1742 Taylor, R. G., and Coauthors, 2013: Ground water and climate change. *Nat. Clim. Chang.*, **3**,  
 1743 322–329, <https://doi.org/10.1038/nclimate1744>.
- 1744 Thomas, B., A. Behrangi, and J. Famiglietti, 2016: Precipitation Intensity Effects on  
 1745 Groundwater Recharge in the Southwestern United States. *Water*, **8**, 90,  
 1746 <https://doi.org/10.3390/w8030090>.
- 1747 Thomas, C. M., B. Dong, and K. Haines, 2020: Inverse modeling of global and regional  
 1748 energy and water cycle fluxes using earth observation data. *J. Clim.*, **33**, 1707–1723,  
 1749 <https://doi.org/10.1175/JCLI-D-19-0343.1>.
- 1750 Tong, X., and Coauthors, 2020: Forest management in southern China generates short term  
 1751 extensive carbon sequestration. *Nat. Commun.*, **11**, 1–10,  
 1752 <https://doi.org/10.1038/s41467-019-13798-8>.
- 1753 Treichler, D., and A. Kääb, 2016: ICESat laser altimetry over small mountain glaciers.  
 1754 *Cryosph.*, **10**, 2129–2146, <https://doi.org/10.5194/tc-10-2129-2016>.
- 1755 Trenberth, K. E., and J. T. Fasullo, 2013: An apparent hiatus in global warming? *Earth's*  
 1756 *Futur.*, **1**, 19–32, <https://doi.org/10.1002/2013ef000165>.
- 1757 —, L. Smith, T. Qian, A. Dai, and J. Fasullo, 2007: Estimates of the global water budget  
 1758 and its annual cycle using observational and model Data. *J. Hydrometeorol.*, **8**, 758–769,  
 1759 <https://doi.org/10.1175/JHM600.1>.
- 1760 —, J. T. Fasullo, and J. Mackaro, 2011: Atmospheric moisture transports from ocean to  
 1761 land and global energy flows in reanalyses. *J. Clim.*, **24**, 4907–4924,  
 1762 <https://doi.org/10.1175/2011JCLI4171.1>.
- 1763 Ukkola, A. M., I. C. Prentice, T. F. Keenan, A. I. J. M. Van Dijk, N. R. Viney, R. B. Myneni,

1764 and J. Bi, 2016: Reduced streamflow in water-stressed climates consistent with CO<sub>2</sub>  
 1765 effects on vegetation. *Nat. Clim. Chang.*, **6**, 75–78,  
 1766 <https://doi.org/10.1038/nclimate2831>.  
 1767 UNESCO, 2020: *World Water Development Report - Water and Climate Change*. 234 pp.  
 1768 United Nations, 2015: *Adoption of the Paris Agreement*. undefined-undefined pp.  
 1769 <https://www.mendeley.com/catalogue/f23ad15f-bf9d-34f1-88c1-8bd56cb2f6c6/>  
 1770 (Accessed September 28, 2020).  
 1771 Vicente- Serrano, S. M., T. R. McVicar, D. G. Miralles, Y. Yang, and M. Tomas- Burguera,  
 1772 2020: Unraveling the influence of atmospheric evaporative demand on drought and its  
 1773 response to climate change. *WIREs Clim. Chang.*, **11**, <https://doi.org/10.1002/wcc.632>.  
 1774 Vinogradova, N., and Coauthors, 2019: Satellite Salinity Observing System: Recent  
 1775 Discoveries and the Way Forward. *Front. Mar. Sci.*, **6**, 243,  
 1776 <https://doi.org/10.3389/fmars.2019.00243>.  
 1777 Voss, K. A., J. S. Famiglietti, M. Lo, C. De Linage, M. Rodell, and S. C. Swenson, 2013:  
 1778 Groundwater depletion in the Middle East from GRACE with implications for  
 1779 transboundary water management in the Tigris-Euphrates-Western Iran region. *Water*  
 1780 *Resour. Res.*, **49**, 904–914, <https://doi.org/10.1002/wrcr.20078>.  
 1781 Wada, Y., L. P. H. Van Beek, and M. F. P. Bierkens, 2012: Nonsustainable groundwater  
 1782 sustaining irrigation: A global assessment. *Water Resour. Res.*, **48**,  
 1783 <https://doi.org/10.1029/2011WR010562>.  
 1784 ———, D. Wisser, and M. F. P. Bierkens, 2014: Global modeling of withdrawal, allocation and  
 1785 consumptive use of surface water and groundwater resources. *Earth Syst. Dyn.*, **5**, 15–  
 1786 40, <https://doi.org/10.5194/esd-5-15-2014>.  
 1787 Wagner, W., and Coauthors, 2013: The ASCAT soil moisture product: A review of its

- 1788 specifications, validation results, and emerging applications. *Meteorol. Zeitschrift*, **22**,  
1789 5–33, <https://doi.org/10.1127/0941-2948/2013/0399>.
- 1790 Wang, S., D. W. McKenney, J. Shang, and J. Li, 2014: A national-scale assessment of long-  
1791 term water budget closures for Canada's watersheds. *J. Geophys. Res. Atmos.*, **119**,  
1792 8712–8725, <https://doi.org/10.1002/2014JD021951>.
- 1793 ———, J. Huang, D. Yang, G. Pavlic, and J. Li, 2015: Long-term water budget imbalances and  
1794 error sources for cold region drainage basins. *Hydrol. Process.*, **29**, 2125–2136,  
1795 <https://doi.org/10.1002/hyp.10343>.
- 1796 Weber, M., L. Braun, W. Mauser, and M. Prasch, 2010: Contribution of rain, snow- and  
1797 icemelt in the upper Danube discharge today and in the future. *Geogr. Fis. e Din. Quat.*,  
1798 **332**, 221–230.
- 1799 Welty, E., and Coauthors, 2020: Worldwide version-controlled database of glacier thickness  
1800 observations. *Earth Syst. Sci. Data Discuss.*, 1–27, [https://doi.org/10.5194/essd-2020-](https://doi.org/10.5194/essd-2020-87)  
1801 87.
- 1802 WGMS, 2020: *Global Glacier Change Bulletin No. 3 (2016-2017)*. G.-  
1803 R.I.N.S.B.J.R.P.P.F.H.M. Zemp M, Ed. IUGG (IACS) / UNEP / UNESCO / WMO,  
1804 World Glacier Monitoring Service,.
- 1805 Whitcher, B., S. D. Byers, P. Guttorp, and D. B. Percival, 2002: Testing for homogeneity of  
1806 variance in time series: Long memory, wavelets, and the Nile River. *Water Resour. Res.*,  
1807 **38**, 12-1-12–16, <https://doi.org/10.1029/2001wr000509>.
- 1808 Willett, K. M., R. J. H. Dunn, J. J. Kennedy, and D. I. Berry, 2020: Development of the  
1809 HadISDH.marine humidity climate monitoring dataset. *Earth Syst. Sci. Data*, **12**, 2853–  
1810 2880, <https://doi.org/10.5194/essd-12-2853-2020>.
- 1811 Williams, A. P., and Coauthors, 2020: Large contribution from anthropogenic warming to an

1812 emerging North American megadrought. *Science* (80-. ), **368**, 314–318,  
 1813 <https://doi.org/10.1126/science.aaz9600>.

1814 Williamson, C. E., J. E. Saros, W. F. Vincent, and J. P. Smol, 2009: Lakes and reservoirs as  
 1815 sentinels, integrators, and regulators of climate change. *Limnol. Oceanogr.*, **54**, 2273–  
 1816 2282, [https://doi.org/10.4319/lo.2009.54.6\\_part\\_2.2273](https://doi.org/10.4319/lo.2009.54.6_part_2.2273).

1817 WMO, 2008: Hydrology-From Measurement to Hydrological Information. *Guide to*  
 1818 *Hydrological Practices*, Vol. 168 of, p. 296.

1819 Wouters, B., A. S. Gardner, and G. Moholdt, 2019: Global glacier mass loss during the  
 1820 GRACE satellite mission (2002-2016). *Front. Earth Sci.*, **7**,  
 1821 <https://doi.org/10.3389/feart.2019.00096>.

1822 WUADAPT, 2020: World Urban Database – World Urban Database and Access Portal  
 1823 Tools. <http://www.wudapt.org/> (Accessed October 8, 2020).

1824 Yang, H., C. Huntingford, A. Wiltshire, S. Sitch, and L. Mercado, 2019: Compensatory  
 1825 climate effects link trends in global runoff to rising atmospheric CO<sub>2</sub> concentration.  
 1826 *Environ. Res. Lett.*, **14**, 124075, <https://doi.org/10.1088/1748-9326/ab5c6f>.

1827 Yebra, M., X. Quan, D. Riaño, P. Rozas Larraondo, A. I. J. M. van Dijk, and G. J. Cary,  
 1828 2018: A fuel moisture content and flammability monitoring methodology for continental  
 1829 Australia based on optical remote sensing. *Remote Sens. Environ.*, **212**, 260–272,  
 1830 <https://doi.org/10.1016/j.rse.2018.04.053>.

1831 Yin, J., X. Zhan, J. Liu, and M. Schull, 2019: An Intercomparison of Noah Model Skills With  
 1832 Benefits of Assimilating SMOPS Blended and Individual Soil Moisture Retrievals.  
 1833 *Water Resour. Res.*, **55**, 2572–2592, <https://doi.org/10.1029/2018WR024326>.

1834 Yu, L., X. Jin, S. A. Josey, T. Lee, A. Kumar, C. Wen, and Y. Xue, 2017: The Global Ocean  
 1835 Water Cycle in Atmospheric Reanalysis, Satellite, and Ocean Salinity. *J. Clim.*, **30**,

1836 3829–3852, <https://doi.org/10.1175/JCLI-D-16-0479.1>.

1837 ———, S. A. Josey, F. M. Bingham, and T. Lee, 2020: Intensification of the global water cycle  
1838 and evidence from ocean salinity: a synthesis review. *Ann. N. Y. Acad. Sci.*, **1472**, 76–  
1839 94, <https://doi.org/10.1111/nyas.14354>.

1840 Zaussinger, F., W. Dorigo, A. Gruber, A. Tarpanelli, P. Filippucci, and L. Brocca, 2019:  
1841 Estimating irrigation water use over the contiguous United States by combining satellite  
1842 and reanalysis soil moisture data. *Hydrol. Earth Syst. Sci.*, **23**, 897–923,  
1843 <https://doi.org/10.5194/hess-23-897-2019>.

1844 Zemp, M., and Coauthors, 2015: Historically unprecedented global glacier decline in the  
1845 early 21st century. *J. Glaciol.*, **61**, 745–762, <https://doi.org/10.3189/2015JoG15J017>.

1846 ———, and Coauthors, 2019: Global glacier mass changes and their contributions to sea-level  
1847 rise from 1961 to 2016. *Nature*, **568**, 382–386, [https://doi.org/10.1038/s41586-019-](https://doi.org/10.1038/s41586-019-1071-0)  
1848 1071-0.

1849 Zhang, J., and Coauthors, 2016a: Multi-Radar Multi-Sensor (MRMS) quantitative  
1850 precipitation estimation: Initial operating capabilities. *Bull. Am. Meteorol. Soc.*, **97**, 621–  
1851 638, <https://doi.org/10.1175/BAMS-D-14-00174.1>.

1852 Zhang, T., R. G. Barry, K. Knowles, J. A. Heginbottom, and J. Brown, 1999: Statistics and  
1853 characteristics of permafrost and ground-ice distribution in the Northern Hemisphere.  
1854 *Polar Geogr.*, **23**, 132–154, <https://doi.org/10.1080/10889370802175895>.

1855 ———, J. A. Heginbottom, R. G. Barry, and J. Brown, 2000: Further statistics on the  
1856 distribution of permafrost and ground ice in the Northern Hemisphere. *Polar Geogr.*, **24**,  
1857 126–131, <https://doi.org/10.1080/10889370009377692>.

1858 Zhang, X., F. W. Zwiers, G. C. Hegerl, F. H. Lambert, N. P. Gillett, S. Solomon, P. A. Stott,  
1859 and T. Nozawa, 2007: Detection of human influence on twentieth-century precipitation



1860 trends. *Nature*, **448**, 461–465, <https://doi.org/10.1038/nature06025>.

1861 Zhang, Y., and Coauthors, 2016b: Multi-decadal trends in global terrestrial  
 1862 evapotranspiration and its components. *Sci. Rep.*, **6**, 1–12,  
 1863 <https://doi.org/10.1038/srep19124>.

1864 Zhang, Y., and Coauthors, 2018: A Climate Data Record (CDR) for the global terrestrial  
 1865 water budget: 1984–2010. *Hydrol. Earth Syst. Sci.*, **22**, 241–263,  
 1866 <https://doi.org/10.5194/hess-22-241-2018>.

1867 Zhou, S., and Coauthors, 2019a: Land–atmosphere feedbacks exacerbate concurrent soil  
 1868 drought and atmospheric aridity. *Proc. Natl. Acad. Sci. U. S. A.*, **116**, 18848–18853,  
 1869 <https://doi.org/10.1073/pnas.1904955116>.

1870 ———, and Coauthors, 2021: Soil moisture–atmosphere feedbacks mitigate declining water  
 1871 availability in drylands. *Nat. Clim. Chang.*, **11**, 38–44, [https://doi.org/10.1038/s41558-](https://doi.org/10.1038/s41558-020-00945-z)  
 1872 [020-00945-z](https://doi.org/10.1038/s41558-020-00945-z).

1873 Zhou, Y., A. H. Sawyer, C. H. David, and J. S. Famiglietti, 2019b: Fresh Submarine  
 1874 Groundwater Discharge to the Near- Global Coast. *Geophys. Res. Lett.*, **46**, 5855–5863,  
 1875 <https://doi.org/10.1029/2019GL082749>.

1876 Zika, J. D., N. Skliris, A. T. Blaker, R. Marsh, A. J. G. Nurser, and S. A. Josey, 2018:  
 1877 Improved estimates of water cycle change from ocean salinity: The key role of ocean  
 1878 warming. *Environ. Res. Lett.*, **13**, 074036, <https://doi.org/10.1088/1748-9326/aace42>.  
 1879  
 1880  
 1881

## Salinity as a proxy for the Ocean Water Cycle

Ocean salinity has long been regarded as a potential rain gauge of the ocean water cycle (Elliott 1974). The cycling of the freshwater between evaporation (E), precipitation (P), and runoff (R) acts in concert with ocean circulation and mixing, driving the salinity distribution to respond to the balance between E, P, and R. Surface waters are generally saltier in the subtropical regions where E exceeds P, and fresher in the tropical and high-latitude regions where P and/or R exceeds E (Schmitt 1995). As the globe warms, the water holding capacity of the atmosphere increases so that more moisture is evaporated from the ocean to the atmosphere. The increased moisture energizes the moisture transport between regions and amplifies the P-E patterns over the ocean. The rate of increase in ocean evaporation is, however, less than the rate predicted by the Clausius-Clapeyron equation, because the global hydrological cycle is constrained by the surface and atmospheric energy budget (e.g. Held and Soden 2006; Hegerl et al. 2015; Allan et al. 2020). Multi-decadal ocean observations showed that mean salinity patterns have amplified, leading to a salinification of the subtropical ocean and freshening of the tropical and high latitude (e.g. Durack and Wijffels 2010). The pattern of change in salinity is consistent with the “dry-gets-drier and wet-gets-wetter” paradigm (Held and Soden 2006), indicating that the oceans hold important insights into the long-term variations of the water cycle and the effects of climate change (Yu et al. 2020). Hence, estimates of the global ocean salt budget change serve as an alternative and independent measure to the change of the freshwater budget in the ocean (Llovel et al. 2019) and is particularly appealing in light of large uncertainties in the present estimates of E, P, and R.

The observed rate of the water cycle intensification inferred from *in situ* salinity observations is about  $8 \pm 5\%$  °C<sup>-1</sup> of global mean surface temperature rise over 1950-2000 (Durack et al. 2012). This rate is in line with theory, but more than twice as large as the rates estimated from state-of-the-art climate models. Several modeling studies have suggested that

the disparity may reflect the effects of ocean warming on the surface salinity pattern amplification in addition to the effects of changing P–E flux arising from the strengthening water cycle (Zika et al. 2018). Ocean warming acts to increase near-surface stratification, prolonging existing salinity contrasts and causing surface salinity patterns to amplify further. Changes in atmospheric circulation patterns alter the locations of the wet and dry portions of the atmospheric circulation, which can also dampen the water cycle change signal passed on to the ocean (e.g. Allan et al. 2020). Hence, the use of ocean salinity as a proxy for P–E should be aware that the processes responsible for the change of ocean salinity may not be as straightforward as a simple response to changes in the P–E field.

Advances in L-band (1.4 GHz) microwave satellite radiometry in the recent decades, pioneered by the ESA’s SMOS and NASA’s Aquarius and SMAP missions, have demonstrated an unprecedented capability to observe global sea surface salinity from space (Vinogradova et al. 2019; Reul et al. 2020). These satellite salinities are complementary to the existing in situ systems such as Argo profiling floats, enabling the salinity observing capability to reach to a depth of 2000 m. It is hoped that the assimilation of satellite and Argo salinities in ocean state estimation and coupled ocean-atmosphere system will lead to advances in estimating the freshwater budget over the global ocean through enforcing ocean dynamical constraints on the changes of P–E as well as R.

1928

## TABLES

1929

Table 1 Summary of water cycle storages including trends. All values in  $10^3 \text{ km}^3$  (storage) or  $10^3 \text{ km}^3 \text{ yr}^{-1}$ 

1930

(trends). Glacier and ice sheets ice weight is calculated to volume by ice density, assuming an ice density of  $917 \text{ kg m}^{-3}$  (IPCC AR5).

1931

3 (IPCC AR5).

Stores	Total volume ( $10^3 \text{ km}^3$ )	Uncertainty (1 sigma)	Uncertainty (%)	Source	Global trends ( $10^3 \text{ km}^3 \text{ yr}^{-1}$ )	Trend uncertainty (95% confidence level:	Source	Type of Observation
Water stored in oceans	1,335,000.0	13,350	1%	<a href="https://ngdc.noaa.gov/mgg/global/etopology_ocean_volumes.html">ngdc.noaa.gov/mgg/global/etopology_ocean_volumes.html</a>	a) 391 (1957-2018) b) 762 (1993-2018) c) 539-666 (GRACE, 2003-2018)	a) +-95 b) +-169	a, b) Frederikse et al. 2020 c) Blazquez et al. 2018	EO, In situ
Water stored in lakes	176.4	26.46	15	Korzoun et al. 1978; Shiklomanov and Rodda 2004	not rated	Not rated	Not rated	EO, In situ
Water stored in d reservoirs	6.4	0.64	10	Shiklomanov 2008	not rated	Not rated	Not rated	EO, In situ
Groundwater	a) 23,400 b) 22,600	16,000-30,000 (range based on porosity uncertainty; Gleeson et al., 2016)	b) 58-133%	a) Oki and Kanae, 2006 b) Gleeson et al., 2016	c) 145 (2000-2008) d) 137 (1960-2010)	c) 39 d) -	c) Konikow 2011 d) de Graaf et al. 2016	Volume based on global lithology and porosity. Trends from EO, in situ and models
Soil moisture	17	Not rated	Not rated	Oki and Kanae, 2006	Not rated	Not rated	Not rated	Reanalysis
Water stored in permafrost a) NH; b) mountain	a) 20.8 b) 0.08	a) 11.1 b) 0.017	a) 53% b) 21%	a) Zhang et al. 2000 b) Jones et al. 2018 (mountain)	Not rated	Not rated	Not rated	In situ, model calculation based on ice content assumptions
Water stored in glaciers	158 (around year 2000)	41	26%	Farinotti et al. (2019, NCEO)	-0.3 (around 2000)	0.1	IPCC SROCC (2019), based on Zemp et al. (2019, Nature), Wouters et al. (2019, Frontiers), and regional studies.	EO, In situ
Water stored in ice sheets	29,200	Not rated	Not rated	Shepherd et al. 2018	-0.472 (2006-2015)	0.024	IPCC SROCC (2019), based on	EO, In situ

and ice shelves							Bamber et al. 2018	
Water stored in snow	3.7	0.5	3-4% (mountains ~10%)	Pulliainen et al. 2020	-0.049 (for 1980-2018.	±0.049 (95% significance)	Pulliainen et al. 2020	EO, In situ
Water stored in vegetation	2.46	0.82	Not rated	This study, based on Tong et al. 2020, Spawn et al. 2020, Penman et al. 2003	Not rated	Not rated	Not rated	EO, In situ
Atmospheric water vapor	12.7	0.3	2-3%	Trenberth et al. 2007	small positive trend	Medium certainty	Chen and Liu 2016	EO, In situ, Reanalysis

1932

**Table 2 Summary of water cycle fluxes including trends. All values in  $10^3 \text{ km}^3 \text{ yr}^{-1}$ .**

Fluxes	ECVs involved	Yearly flux ( $10^3 \text{ km}^3 \text{ yr}^{-1}$ )	Uncertainty (1sigma)	Uncertainty (%)	Reference	Global trends ( $10^3 \text{ km}^3 \text{ yr}^{-2}$ )	Trend uncertainty	reference	Type of Observation
Precipitation over land	Precipitation	(a) 123.3 (b) 116.5	(a) 5.4 (b) 5.1	(a) 4.4% (b) 4.4%	(a) Koutsoyiannis, et. al 2020, (b) Rodell et al. 2015	Currently not detectable outside of noise	Not rated	Not rated	EO, In situ, Reanalysis
Precipitation over ocean	Precipitation	(a) 399.4 (b) 403.5	(a) 22.0 (b) 22.1	(a) 5.5% (b) 5.5%	(a) Koutsoyiannis, et. al 2020, (b) Rodell, et al., 2015	Currently not detectable outside of noise	Not rated	Not rated	EO, In situ, Reanalysis
Land evaporation	Evaporation from land	69.2	7.0	10%	Miralles et al. (2016)	0.29	0.15	Pan et al. 2020	EO, In situ, Reanalysis
Evaporation over ocean	evaporation	450.8	31.1	7%	Yu et al. 2017	0.66	0.20	Yu et al. 2020	EO, In situ, Reanalysis
Atmospheric moisture transport from ocean to land	TCWV	45.8	4.4	9.6%	Rodell et al. 2015, Schneider et al. 2017	Not rated	Not rated	Not rated	Reanalysis
River discharge	river discharge	a) 38.5 b) 39.8	1.5	~4%	a) Ghiggi et al. 2019 b) Schmied et al 2020	Not rated	Not rated	Not rated	In situ + model
Groundwater discharge (fresh)	Groundwater	0.5	0.3	60%	Zhou et al. 2019	Currently not detectable outside of noise	Not rated	Not rated	In situ + model
Groundwater recharge	Groundwater	13.6	0.9	~13%	Mohan et al. 2018	Not rated	Not rated	Not rated	Model, validated with in-situ data

Glacier turnover a) 1961-1990 b) 1980-2012	Glacier	a) 0.436 b) 0.916	a) 0.273 b) 0.273	a) 64% b) 32%	a) Braithwaite and Hughes 2020 b) Huss and Hock 2015 Both studies estimate the flux from modelling. Numbers are a combination of both flux and change in storage. Density ass. 919 kg m <sup>-3</sup> .	Not rated	Not rated	Not rated	EO, In situ, Reanalysis
Ice sheet turnover a) West Antarctic, b) East Antarctic, c) Greenland ice sheet	Ice sheet	(a+b) - 0.169 c) -0.303 (2006-2015), (a+b) - 0.089 c) -0.287 (2002-2011)	(a+b) 0.021 c) 0.012 (2006-2015), (a+b) 0.029 c) 0.023 (2002-2011)	Not rated	IPCC 2019	(a+b) - 0.089 to -0.169, (c) -0.287 to -0.303 for (2002-2011) to (2006-2015)	Not rated	Not rated	EO, In situ,
Permafrost water turnover	Permafrost	4.3	Not rated	Not rated	Shiklomanov et al. 2021	+0.250 (1936-2015)	Not rated	Shiklomanov et al. 2021	In situ, reanalysis
ground water extraction a) flux-based method b) volume-based	Anthropogenic water use	a) 0.20 b) 0.15	a) 0.03 b) 0.04	Not rated	Taylor et al. 2013	Not rated	Not rated	Not rated	EO, In situ, Reanalysis
Blue Water Irrigation	Anthropogenic water use	2.7	Not rated	Not rated	FAO 2021	Not rated	Not rated	Not rated	National reporting
Domestic and industrial blue water use	Anthropogenic water use	1.3	Not rated	Not rated	Flörke et al. 2013	+0.02	Not rated	Flörke et al. 2013	Modelling

1933

Table 3 Summary capability demands and outlook of water cycle storages

Storage	Observational needs		Observational outlook		Other (methodological developments, reanalysis, etc.)
	in situ	EO	in situ	EO	
Oceans	Enhance the Argo array of profiling floats including full-depth Argo to estimate the contribution of deep-ocean warming and salinity changes.	Ensure the continuity of satellite altimetry beyond 2030; ensure the continuity of satellite gravimetry and surface salinity missions	Establishment of a fully global, top-to-bottom, dynamically complete, and multidisciplinary Argo Program	Constellation of satellite altimetry for sea level and satellite radiometry for sea surface salinity. The CIMR mission concept can provide continuity for satellite salinity measurements	A suite of ocean reanalysis products that assimilate various in-situ and EO measurements for ocean ECVs. In the future Argo will integrate seamlessly with satellite and with other <i>in situ</i> elements.

Terrestrial Open Water (Lakes, artificial reservoirs, wetlands)	Determine the exact quantity of water from lakes and wetlands that contribute to global closure of the water cycle; more precise and more frequent updates of hypsometry curves needed	Ensure the continuity of high-resolution satellite altimetry beyond 2030		SWOT mission for characterization or water table depth of smaller lakes; Sentinel 1 and 2 satellites will greatly complement existing series of Landsat images used for hypsometry curves	Focus on a set of representative lakes that most objectively reflect the climatic signal
Atmospheric water vapor	More in-situ measurements are needed over oceans and in the Southern Hemisphere	Improved satellite-based measurements to measure water vapor over land during cloudy conditions, in the lower troposphere and the boundary layer. Dedicated mission for moisture convergence monitoring	Increased number of frost point hygrometer launch sites as part of the GRUAN network.	CrIS and ATMS instruments for JPSS-3 and JPSS-4. IASI-NG, METImage, MWI, and MWS on EPS-SG, AMSR-3 on GOSAT-GW.	Reanalysis models must be improved to maintain water mass balance
Groundwater	Maintain and extend in-situ national groundwater level monitoring networks to close observational gaps (particularly in the Global South) and promote data sharing among countries.	Higher spatial resolution to monitor smaller aquifers; long-term observing system	Establishment of new national groundwater monitoring programmes.	Next-generation global gravity satellite missions with increased spatial resolution planned	Improved modelling and downscaling of groundwater variations using machine learning
Soil moisture	Expand capabilities to underrepresented regions (e.g. Africa, Southern America) and climates that are currently poorly covered (e.g. monsoon, tropic, polar); clever, dense network design to bridge scale gaps	Continuation of dedicated L-band soil moisture missions; improved spatial resolution	Establishment of fiducial reference networks (ESA, Copernicus)	CIMR L-band, Tandem-L, Rose L, HydroTerra for diurnal variability, high-resolution products from downscaling and SAR satellites	Better retrievals and models for dense vegetation and organic soils
Glaciers	Additional multi-temporal glacier inventories every ~20 years; better spatial coverage of glacier thickness measurements; at least one long-term mass-balance monitoring program in every larger mountain range providing glaciological variability at seasonal to annual time resolution	close geodetic gaps in regions where glaciers dominate runoff during warm/dry seasons, e.g. in the tropical Andes and in Central Asia, and in the heavily glacierized regions dominating the glacier contribution to sea-level rise, i.e. Alaska, Arctic Canada, Russian Arctic, Greenland and Antarctica.		spaceborne altimetry (ICESat-2); increasing availability of large-scale high-resolution DEMs; Unlock national archives of aerial surveys and photogrammetric processing of early optical satellite data;	Exploit reconstructions from topographic maps and geomorphological evidence
Ice sheets and ice shelves	International coordinated observation flight campaigns to cover the “missing areas” along major outlet glaciers,	Continuation and effective combination of various existing satellite programs, e.g. ICESat-2, CryoSat and future	Campaigns in Greenland and Antarctica for satellite validation. Need to close observational gap	ESA Crystal mission, Copernicus CMIR, CRISTAL, (Copernicus Polar Ice and Snow	Need of more diverse atmosphere reanalysis products, e.g., snow densities, firm compactions, snow drift and surface conditions, to narrow down ice

	particularly in East Antarctica. Surface traverse campaigns for improving firm models and englacial hydrology, especially in Greenland with its increasing seasonal melt zones	ESA Crystal missions	with unknown outlet glacier thickness in East Antarctica	Topography Altimeter) and ROSE-L	sheet mass change models
Permafrost	The main difficulty for assessing permafrost distribution, ice content and mass changes is that permafrost is not visible at the surface.	Still no reliable remote sensing technique for detecting permafrost Need for a surface subsidence product	Spatial observational gaps have to be filled.	Tentatives are in progress within the ESA/CCI project	Most urgent need is a sustainable and reliable funding of monitoring networks and the database infrastructure, ensuring long-term availability of observational data.
Snow	expand ground-based observation networks	continuation of satellite programs		CIMR is expected to provide SWE at improved accuracy and resolution; SAR based approaches (e.g., Sentinel-1) for mapping snow mass and SWE in mountain areas	fusing observations from active and passive sensors or combining them with independent reference data

1934

1935



Table 4 Summary capability demands and outlook of water cycle fluxes

Flux	Observational needs		Observational outlook		Other methodological developments, reanalysis, etc.
	in situ	EO	in situ	EO	
Ocean evaporation	near-surface observations with focus on air temperature and humidity	improved satellite retrieval algorithms for near-surface ECVs with focus on air temperature and humidity	Explore the use of air-sea observations from new autonomous platforms such as saildrones and wave gliders; sustained and expand existing surface buoy network	Continuity of microwave imager programmes via, e.g., EUMETSAT (EPS-SG) and JAXA (GOSAT-GW) and NOAA JPSS (ATMS)	Improvement of the model constraint of the ocean E-P estimates and the model-data synthesis capability of EO to the ocean water cycle; reconcile large spread in atmospheric reanalysis models and satellite gridded products
Land evaporation	Novel means to measure interception loss over multiple ecosystems	Missions dedicated to measuring evaporation to improve water budget closure over tropical, semiarid and high-latitude areas	Use of data from new in situ networks such as SAPFLUXNET ( <a href="http://sapfluxnet.creaf.cat">http://sapfluxnet.creaf.cat</a> ) in combination with eddy-covariance data	New types of EO (such as solar induced chlorophyll fluorescence) and new platforms (such as CubeSats and UAVs)	
Ocean precipitation		Retrieval skills need to be improved, to address intermittent nature and high spatial and temporal variability of precipitation		Continuity of microwave imager and sounder programmes via, e.g., EUMETSAT (EPS-SG), JAXA (GOSAT-GW) and NOAA (JPSS); NASA-JAXA PMM; improved snow retrieval capabilities with ICI (EUMETSAT, EPS-SG), largely improved temporal sampling with the TROPICS mission (NASA)	Integration of multiple sensors and deriving reanalysis products will address the high spatial and temporal variability
Land precipitation	Improve timeliness to contribute precipitation data to GPCC	Improved consistent long-term datasets;		Same as for ocean precipitation	Integration of multiple sensors (in situ, remote sensing) and techniques (rain gauges, meteorological radars, soil moisture).
River discharge	Improve timeliness to contribute data to GTN-R. Long-term, regular measurements of upstream river discharge on finer spatial scale	Increase numbers of virtual stations from altimetry	In situ observations are globally under threat due to reduced field observation capabilities and priorities.	SWOT for measuring rivers wider than 100 meters. SWOT assimilation into models to derive first globally consistent information on river discharge	Data integration and assimilation methods will be used to provide information on river discharge based on different sensors and observation techniques.
Groundwater discharge from continents to ocean	Increase number and frequency of observations	Better understanding of usefulness of EO for groundwater discharge monitoring	Advances in geophysical tools, which can be coupled with hydrological flow modeling.		Model simulations are becoming more skillful due to increasing

	of groundwater discharge.				availability of high-quality hydrologic and topographic data that feed them.
Glacier and ice sheet turnover	To understand rapid changes in ice mass flux and ice instability the observation of bottom melting is essential.		Close coordination as diverse as earth rheology and geophysics (for heat flow modelling), glaciology for understanding ice movements, crevassing and calving, meteorology for snowfall and firn compaction is required.	Broadband observation from visual to L-band radar active measurements, and passive microwave observations sensitive to surface melting	Improved estimations of glacier mass turnover require a better integration of observations into numerical models with full representation of individual glaciers
Anthropogenic water use	Irrigation surveys available at sub-national scale, with shorter delivery time	Improved spatial and temporal resolution of microwave observations for soil moisture retrieval.		The revisit time will improve after launch of two new Sentinels, i.e. Sentinel-1C and Sentinel-1D, planned for 2022 and 2023. ESA Earth Explorer Hydroterra for sub-daily observations	Downscaling of coarse satellite soil moisture to resolve elements of anthropogenic water use; integrated modelling approaches for resolving anthropogenic water use at the necessary scale and temporal resolution, with accounting and satellite data used for input and validation.

1937

1938

## A1 Summary of (semi-)operational long-term global observing systems and programs of water cycle storages

Storage	GCOS ECVs involved	in situ	EO
Oceans	sea level, sea surface and subsurface temperature, (Suggested as possible future ECV: ocean mass, ocean bottom pressure)	GLOSS - Global Sea-Level Observing System ( <a href="http://gloss-sealevel.org/data/">gloss-sealevel.org/data/</a> )  International Comprehensive Ocean-Atmosphere Data Set (ICOADS) ( <a href="http://rda.ucar.edu/datasets/ds548.0/">rda.ucar.edu/datasets/ds548.0/</a> );  UKMO EN4 subsurface temperature and salinity ( <a href="http://metoffice.gov.uk/hadobs/en4/">metoffice.gov.uk/hadobs/en4/</a> )	JPL PODAAC: ( <a href="http://podaac.jpl.nasa.gov/OceanSurfaceTopography/">podaac.jpl.nasa.gov/OceanSurfaceTopography/</a> );  ESA CCI Sea Level ( <a href="http://climate.esa.int/odp/">climate.esa.int/odp/</a> );  ESA CCI Sea Surface Temperature ( <a href="http://climate.esa.int/odp/">climate.esa.int/odp/</a> );  Copernicus Marine Service ( <a href="http://marine.copernicus.eu/">marine.copernicus.eu/</a> );  Group for High Resolution Sea Surface Temperature ( <a href="http://ghrsst.org/">ghrsst.org/</a> );  Hydroweb ( <a href="http://legos.obs-mip.fr/soa/hydrologie/hydroweb/">legos.obs-mip.fr/soa/hydrologie/hydroweb/</a> ) as part of GTN-H)
Lakes and reservoirs	Lakes	International Data Centre on Hydrology of Lakes and Reservoirs ( <a href="http://hydrolare.net/">hydrolare.net/</a> ) hosts the GTN-L as part of GTN-H	ESA CCI Lakes ( <a href="http://climate.esa.int/odp/">climate.esa.int/odp/</a> ) Copernicus Global Land Surface ( <a href="http://land.copernicus.eu/">land.copernicus.eu/</a> )
Atmospheric water vapor	Water Vapor	Hadley Centre Integrated Surface Database (HadISD) ( <a href="http://metoffice.gov.uk/hadobs/hadis/">metoffice.gov.uk/hadobs/hadis/</a> );  International Comprehensive Ocean-Atmosphere Data Set (ICOADS) ( <a href="http://rda.ucar.edu/datasets/ds548.0/">rda.ucar.edu/datasets/ds548.0/</a> );  Integrated Surface Database (ISD) of the NCEI of NOAA ( <a href="http://ncdc.noaa.gov/isd/data-access">ncdc.noaa.gov/isd/data-access</a> )	Copernicus Atmosphere Monitoring Service ( <a href="http://atmosphere.copernicus.eu/">atmosphere.copernicus.eu/</a> )  EUMETSAT CM SAF ( <a href="http://cmsaf.eu">cmsaf.eu</a> )  ESA CCI Water Vapour ( <a href="http://climate.esa.int/odp/">climate.esa.int/odp/</a> )  Remote Sensing Systems ( <a href="http://remss.com">remss.com</a> )
Groundwater	Groundwater	Global Groundwater Monitoring Network ( <a href="http://un-igrac.org/special-project/ggmn-global-groundwater-monitoring-network">un-igrac.org/special-project/ggmn-global-groundwater-monitoring-network</a> ) hosted by IGRAC and part of GTN-H	none
Soil moisture	Soil moisture	International Soil Moisture network and part of GTN-H ( <a href="http://ismn.geo.tuwien.ac.at/">ismn.geo.tuwien.ac.at/</a> ; <a href="http://ismn.earth">ismn.earth</a> )	ESA CCI Soil Moisture ( <a href="http://climate.esa.int/odp/">climate.esa.int/odp/</a> );  C3S soil moisture ( <a href="http://cds.climate.copernicus.eu/">cds.climate.copernicus.eu/</a> );
Permafrost	Permafrost	Global Terrestrial Network – Permafrost (GTN-P)	none
Glaciers	Glaciers	US National Snow and Ice Data Center ( <a href="http://nsidc.org">nsidc.org</a> ) as part of GTN-G ( <a href="http://gtm-g.org">gtm-g.org</a> );  World Glacier Monitoring Service ( <a href="http://wgms.ch">wgms.ch</a> ) as part of GTN-G ( <a href="http://gtm-g.org">gtm-g.org</a> );	US National Snow and Ice Data Center ( <a href="http://nsidc.org">nsidc.org</a> );  World Glacier Monitoring Service ( <a href="http://wgms.ch">wgms.ch</a> ) as part of GTN-G ( <a href="http://gtm-g.org">gtm-g.org</a> );  ESA CCI Glaciers ( <a href="http://climate.esa.int/odp/">climate.esa.int/odp/</a> )
Ice sheets and ice shelves	Ice sheets and ice shelves	National Snow and Ice Data Center ( <a href="http://nsidc.org">nsidc.org</a> )  PROMICE ( <a href="http://promice.dk">promice.dk</a> )	Satellite ECV Inventory by the CEOS/CGMS Working Group on Climate (WGClimate) ( <a href="http://climatemonitoring.info/ecvinventory/">climatemonitoring.info/ecvinventory/</a> );  ESA CCI Greenland and Antarctica Ice Sheets ( <a href="http://climate.esa.int/odp/">climate.esa.int/odp/</a> );  C3S ice sheets ( <a href="http://cds.climate.copernicus.eu/">cds.climate.copernicus.eu/</a> );
Snow	Snow	National Snow and Ice Data Center ( <a href="http://nsidc.org/">nsidc.org/</a> );  Global Snow Lab ( <a href="http://climate.rutgers.edu/snowcover/">climate.rutgers.edu/snowcover/</a> )	ESA CCI Snow ( <a href="http://climate.esa.int/odp/">climate.esa.int/odp/</a> )  Copernicus Global Land Service ( <a href="http://land.copernicus.eu">land.copernicus.eu</a> )
Living biomass	Above-ground biomass	None	ESA Globbiomass ( <a href="http://globbiomass.org/">globbiomass.org/</a> ); ESA CCI Biomass project ( <a href="http://climate.esa.int/odp/">climate.esa.int/odp/</a> ); NASA Carbon Monitoring Systems ( <a href="http://carbon.nasa.gov/">carbon.nasa.gov/</a> )

Flux	GCOS ECVs involved	in situ	EO
Ocean evaporation	Sea surface temperature; wind speed; air temperature; air humidity	GLOSS - Global Sea-Level Observing System ( <a href="http://sealevel.org/data/">gloss-sealevel.org/data/</a> );  International Comprehensive Ocean-Atmosphere Data Set (ICOADS) ( <a href="http://rda.ucar.edu/datasets/ds548.0/">rda.ucar.edu/datasets/ds548.0/</a> )	JPL PODAAC ( <a href="http://podaac.jpl.nasa.gov/OceanSurfaceTopography">podaac.jpl.nasa.gov/OceanSurfaceTopography</a> ) CM SAF ( <a href="http://10.5676/EUM_SAF_CM/HOAPS/V002">10.5676/EUM_SAF_CM/HOAPS/V002</a> )  ESA CCI Sea Level ( <a href="http://climate.esa.int/odp">climate.esa.int/odp</a> );  ESA CCI Sea Surface Temperature ( <a href="http://climate.esa.int/odp">climate.esa.int/odp</a> );  SEAFLUX ( <a href="http://seafux.org">http://seafux.org</a> ) Cross-calibrated multiplatform (CCMP) gridded surface vector winds ( <a href="http://www.remss.com">http://www.remss.com</a> )  Copernicus Marine Service ( <a href="http://marine.copernicus.eu/">marine.copernicus.eu/</a> )
Land evaporation	Evaporation from Land	FLUXNET ( <a href="http://fluxnet.ornl.gov">fluxnet.ornl.gov</a> ) SAPFLUXNET ( <a href="http://sapfluxnet.creaf.cat">http://sapfluxnet.creaf.cat</a> )	MOD16 ( <a href="http://ladsweb.modaps.eosdis.nasa.gov/search/order/2/MOD16A2--6">ladsweb.modaps.eosdis.nasa.gov/search/order/2/MOD16A2--6</a> );  Global Land Evaporation Amsterdam Model (GLEAM; <a href="http://gleam.eu">gleam.eu</a> );
Ocean precipitation	Precipitation	OceanRAIN ( <a href="http://oceanrain.cen.uni-hamburg.de/">oceanrain.cen.uni-hamburg.de/</a> )	GPCP ( <a href="http://psl.noaa.gov">psl.noaa.gov</a> );  PERSIANN ( <a href="https://data.nodc.noaa.gov/">https://data.nodc.noaa.gov/</a> );  IMERG ( <a href="http://gpm.nasa.gov/">gpm.nasa.gov/</a> )  CM SAF (HOAPS CDRs ( <a href="http://10.5676/EUM_SAF_CM/HOAPS/V002">10.5676/EUM_SAF_CM/HOAPS/V002</a> ))  IPWG at <a href="http://www.isac.cnr.it/~ipwg/data/datasets.html">http://www.isac.cnr.it/~ipwg/data/datasets.html</a>
land precipitation	Precipitation	GPCC ( <a href="http://opendata.dwd.de/climate_environment/GPCC/html/download_gate.html">opendata.dwd.de/climate_environment/GPCC/html/download_gate.html</a> );  Integrated Surface Database (ISD) of NCEI-NOAA ( <a href="http://ncdc.noaa.gov/isd/data-access">ncdc.noaa.gov/isd/data-access</a> );  Global Historical Climatology Network (GHCN) of NCEI-NOAA ( <a href="http://ncdc.noaa.gov/data-access/land-based-station-data/land-base">ncdc.noaa.gov/data-access/land-based-station-data/land-base</a> )	As for ocean precipitation
River discharge	River discharge	WMO Hydrological Observing System ( <a href="http://wmo.int/pages/prog/hwrrp/chy/whos/index.php">wmo.int/pages/prog/hwrrp/chy/whos/index.php</a> )  Global Runoff Data Base (GRDC) ( <a href="http://portal.grdc.bafg.de/">portal.grdc.bafg.de/</a> );  The Global River Discharge (RivDIS) Project ( <a href="http://rivdis.sr.unh.edu">rivdis.sr.unh.edu</a> )	None
Groundwater discharge	Groundwater	None	None
Glacier and ice sheet turnover	Glaciers; Ice sheets and ice shelves	None	None
Anthropogenic use		FAO AQUASTAT ( <a href="http://fao.org/aquastat/en/databases/">fao.org/aquastat/en/databases/</a> ) as part of GTN-H	None

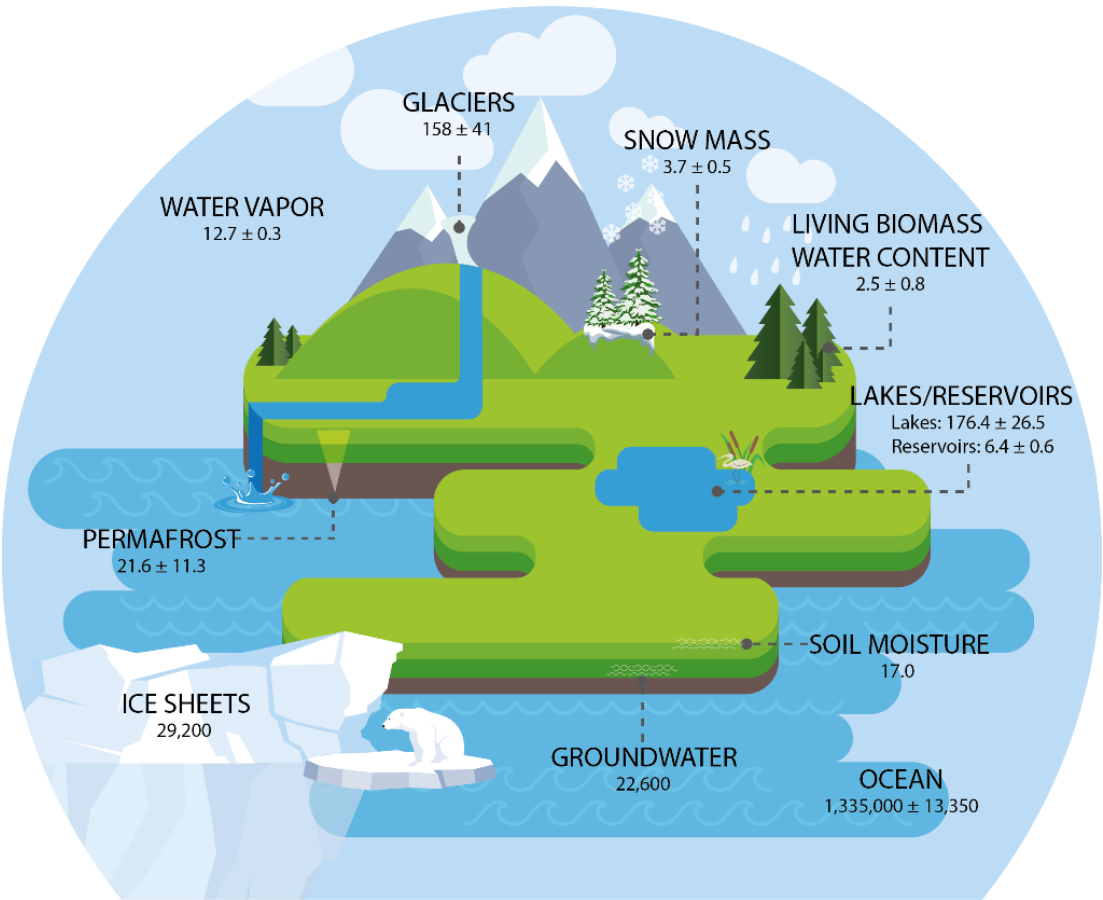
1943 **A3 Summary of observation-based large-scale water cycle studies. EO means that multiple satellite observations**  
 1944 **are used for the same water component to quantify the uncertainty in these.**

Reference	Temporal resolution	Spatial resolution	Spatial domain	Temporal domain	Objective	Input data	Combination method
Rodell et al. 2004	Monthly	1 basin Mississippi	Regional	14 months	Estimate ET from GRACE	EO, In situ, Reanalysis	No optimization Land
Rodell et al. 2011	Monthly	7 basins	Global	8 years	Estimate ET uncertainty	EO, In Situ, Reanalysis	No optimization Land
Azardeakhsh et al. 2011	Monthly	Multiple sub-basins over the Amazon	Regional	4 years	Estimate river discharge & spatial analysis	EO, In situ	No optimization Land
Hirschi & Seneviratne 2017	Monthly	341 basins	Global	20 years	Long-term estimation of change in storage	In situ, Reanalysis	No optimization Land+Atmosphere
Mariotti et al. 2002	Climatology	Basin and pixel over Mediterranean	Regional	20 years	Estimation Gibraltar strait netflow	EO, In situ, Reanalysis	No optimization Ocean+Atmosphere
Sheffield et al. 2009	Monthly	1 basin Mississippi	Regional	2 years	Water budget imbalance	EO, In situ	No optimization Land
Moreira et al. 2019	Monthly	Basin and pixel over South Amer.	Continental	10 years	Water budget imbalance	EO, In situ	No optimization Land
Rodell et al. 2015	Climatologic season	Continental	Global	10 years	Optimize global fluxes	EO, In situ, Reanalysis, Model	Optimal interpolation Land+Atm.+Ocean With energy cycle
Pan et al. 2012	Monthly	32 basins	Global	20 years	Optimize long-term fluxes	EO, In situ, Reanalysis, Model	Assimilation Land
Pellet et al. 2019	Monthly	Sub-basins over Mediterranean	Regional	8 years	Optimize regional water cycle	EO, In situ, Reanalysis	Optimal interpolation Land+Atm.+Ocean
Munier & Aires 2018	Monthly	9 basins	Global	8 years	Optimize and error analysis	EO, In situ	Optimal interpolation Land
Sahoo et al. 2011	Monthly	10 basins	Global	3 years	Optimize using satellite only data	EO, In situ, Model	Assimilation Land
Shiklomanov et al. 2021	Seasonal	Basins	Pan-Arctic	30-50 years	Estimate change in river discharge	In situ	
Zhang et al. 2018	Monthly	0.5° Pixel	Global	25 years	Climate data record	EO, Model	Zhang et al. 2016

1946

1947

FIGURES



GLOBAL WATER STORAGES

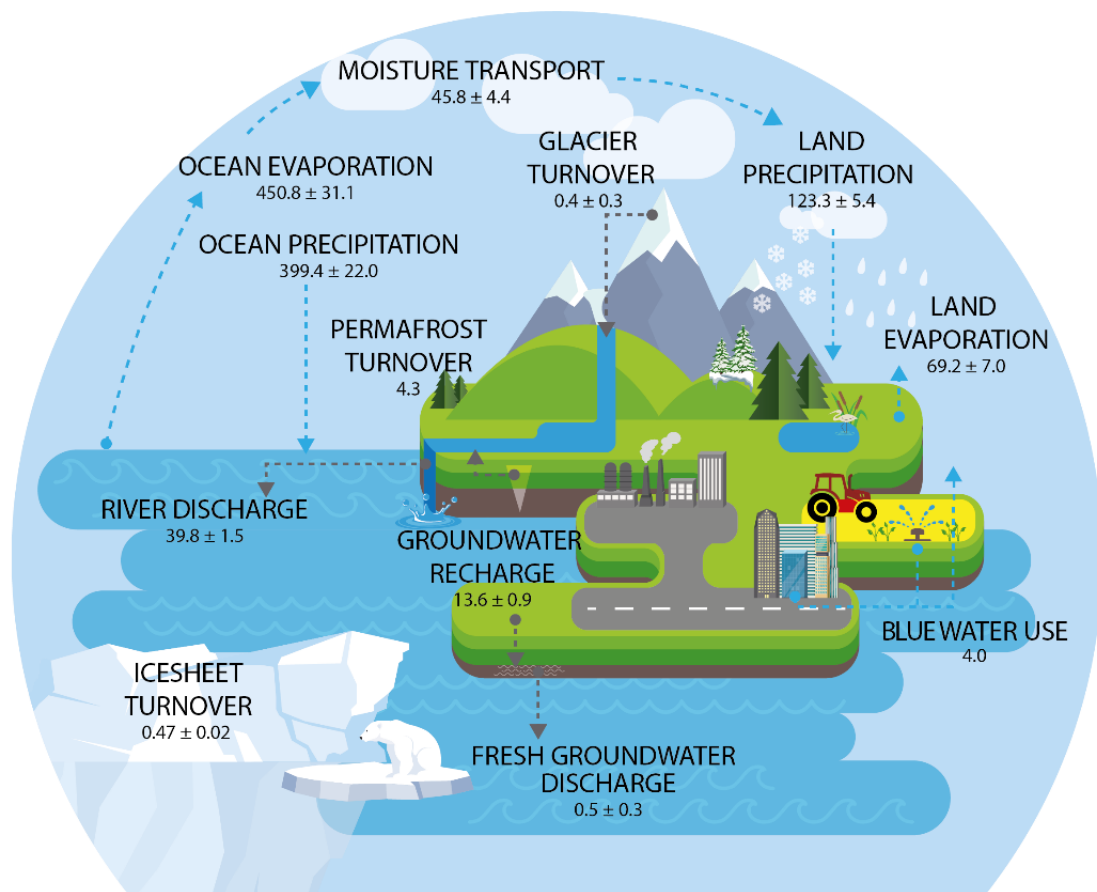
1948

1949

1950

1951

Figure 1 Observed estimates of global water cycle storages (in  $10^3 \text{ km}^3$ ) and their uncertainties. Sources of individual estimates are reported in Table 1.



## GLOBAL WATER CYCLE FLUXES

1952

1953

**Figure 2** Observed estimates of annual global water cycle fluxes (in  $10^3 \text{ km}^3$ ) and their trends. Sources of individual estimates are reported in Table 2

1954

1955